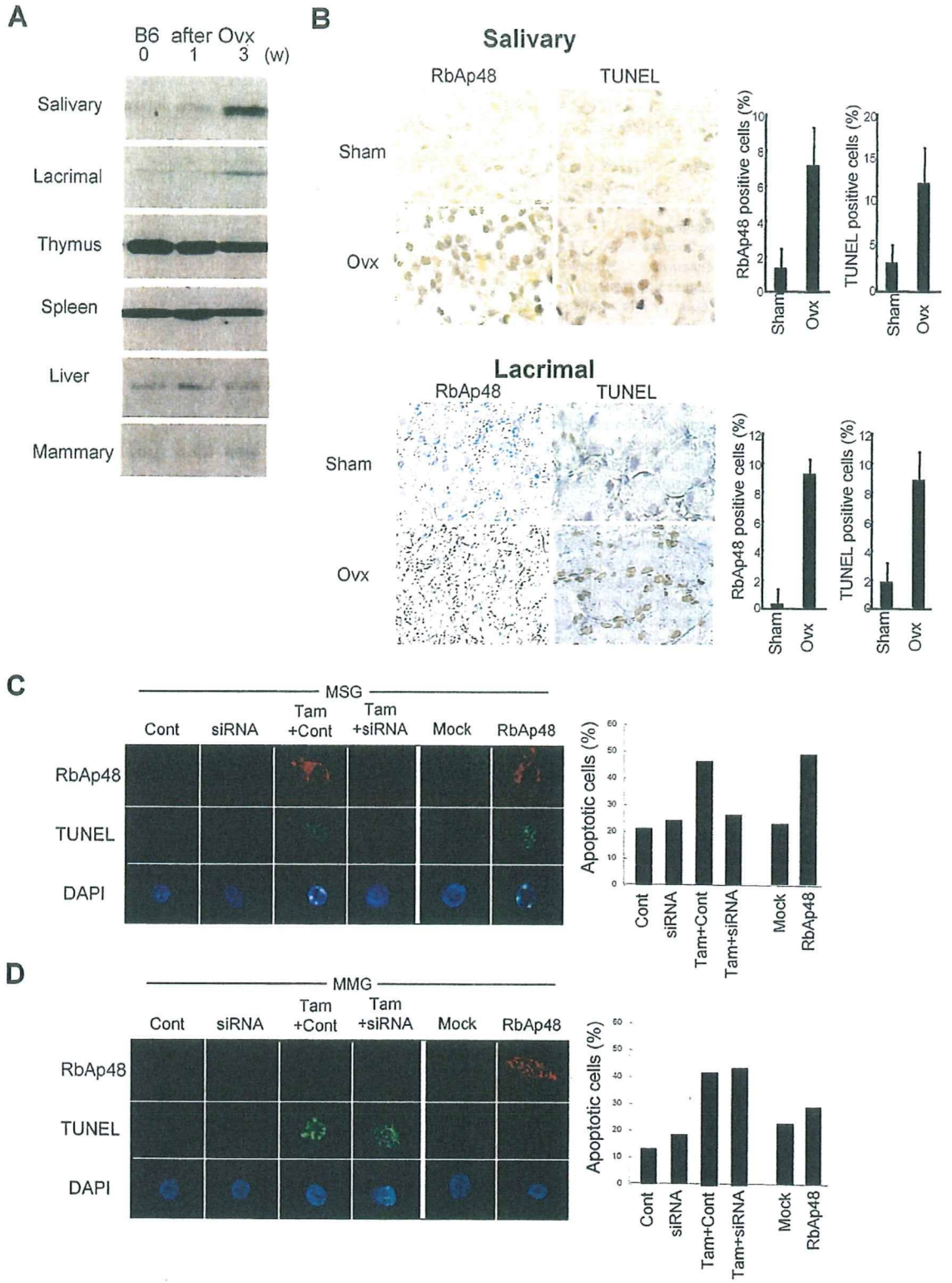

FIG. 2. RbAp48 overexpression in OVX B6 mice. (A) Increased RbAp48 expression in salivary and lacrimal gland tissues in OVX B6 mice from 0 to 3 weeks (age of mice, 4 to 7 weeks). Expression levels of RbAp48 in thymus, spleen, liver, and mammary glands from OVX B6 mice were constant. Western blot analysis was performed on proteins from tissue homogenates of OVX and sham mice. Blots were representative of three independent experiments. (B) Detection of RbAp48^{+} and TUNEL^{-} cells in salivary and lacrimal glands from OVX B6 and sham B6 mice at the age of 7 weeks. Immunohistochemical analysis of RbAp48 and in situ TUNEL assays were performed on the sections of salivary and lacrimal glands from OVX and sham mice. Images are representative of sections from five mice. The percentage of RbAp48^{+} and TUNEL^{+} cells in salivary and lacrimal glands was enumerated using a 10- by 20-mm grid covering an objective area of 0.16 mm^2. Data were analyzed in 10 fields per section and expressed as mean percent ± standard deviation of data from five mice. (C) TAM-induced apoptosis was associated with RbAp48 expression in

rials were then digested for 1 h at 37°C with 750 U/ml collagenase (Wako), 500 U/ml hyarulonidase type IV (Sigma), 1% bovine serum albumin, and 10 mM HEPES (pH 7.4) in DMEM. After digestion, they were filtered through a 70-μm nylon mesh, centrifuged, and rinsed twice with DMEM containing 10% FCS. These cells were cultured in chamber slides (Nalge Nunc International, Denmark) at a density of 5×10^4/well with DMEM containing 10% FCS. After cells were cultured for 24 h, the medium was changed to HuMedia-KG2 (Kurabo, Osaka, Japan).

Differential display analysis and Northern blotting. Total RNA was isolated from TAM-treated or nontreated HSG cells and reverse transcribed for differential display PCR with an RNAimage kit (Gene Hunter, Nashville, TN). TAM-induced cDNA fragments were gel excised and subcloned for TA vector. The clones were screened with a cDNA library derived from mRNA of TAM-stimulated HSG cells. The screened clone was transformed to plasmid and sequenced. Expressions of RbAp48 mRNA were detected by Northern blot analysis using ^{32}P-labeled RbAp48 cDNA probe. Equal loading of the gel was confirmed by using β-actin cDNA probe. In addition, the human total RNA-blotted membrane (Biocain Institute, Inc., San Leandro, CA) was used for analysis of RbAp48 mRNA in various human tissues.

Apoptosis detection assay. Apoptosis was detected using the annexin V-fluorescein isothiocyanate (FITC) apoptosis detection kit (Genzyme Corp., Cambridge, MA). Briefly, after cultured cells were washed with phosphate-buffered saline, the cells were incubated with FITC-conjugated annexin V and propidium iodide (PI) for 10 min at room temperature in the dark. Binding buffer was added, and apoptotic cells were detected by flow cytometric analysis with an EPICS flow cytometer (Beckman Coulter, Inc., Miami, FL).

Mice. Estrogen receptor α-deficient ($ER\alpha^{-/-}$), $p53^{-/-}$, $E2F\text{-}1^{-/-}$, or C57BL/6 (B6) mice were purchased from Taconic (Germantown, NY), Jackson Laboratory (Bar Harbor, ME), or Nihon Clea (Tokyo, Japan). These mice were subjected to ovariectomy (OVX mice) and or to a sham operation (sham mice) at 4 weeks of age. At 0 to 3 weeks after OVX, all organs were evaluated by pathological or immunohistochemical analysis. To generate the RbAp48-transgenic (TG) mice, B6 mice were used to obtain fertilized eggs, and the gene fragment containing RbAp48 cDNA regulated by salivary gland-specific promoter (22) (provided by B. B. Larsen) was microinjected into the pronucleus of fertilized eggs to establish the transgenic lines. Histopathological analysis of all organs of RbAp48-TG mice screened by PCR was performed. All mice were maintained in our specific-pathogen-free facility.

siRNA of RbAp48. Small interfering RNA (siRNA) corresponding to the coding sequence +136 to +156 of the RbAp48 gene was synthesized by Hokkaido System Science (Sapporo, Japan) according to standard methods (23, 52) for the following: sense, CGAGGAAUACAAAAUAUGGTT; antisense, CCA UAUUUUGUAUUCCUCGTT. siRNA of the glyceraldehyde-3-phosphate dehydrogenase (GAPDH) gene (Ambion, Austin, TX) was used as a control. siRNA (0 to 50 nM) and 1 μg of pCMV-green fluorescent protein (GFP) plasmid were cotransfected into HSG, MCF-7 cells, and the IPTG-controlled RbAp48-stable cell line (RH0) using a Silencer siRNA Transfection II Kit (Ambion) or FuGENE6 (Roche). At 24 h after cotransfection, RH0 cells were incubated with IPTG for an additional 24 h. GFP^+ apoptotic cells were detected by flow cytometry using phycoerythrin (PE)-conjugated annexin V.

E2F-1, ARF, and p53 siRNA. For siRNA of E2F-1, ARF, and p53, an siTrio Full Set (B-Brigde International, Sunnyvale, CA) was used for HSG cells. Briefly, each cocktail including the three RNA oligonucleotides listed below was transfected into cells with a Quick-Step Transfection Kit (B-Brigde International). Sequences of the oligonucleotide sets are as follows: for E2F-1, CCAACGUCCU UGAGGGCAUTT (sense), AUGCCCUCAAGGACGUUGGTT (antisense), CU GCAGAGCAGAUGGUUAUTT (sense), AUAACCAUCUGCUCUGCAGTT (antisense), GGAAAGUGAGGGAGGGAGATT (sense), and UCUCCCUCCC UCACUUUCCTT (antisense); for ARF, GCUCACCUCUGGUGCCAAATT (sense), UCACCAAGAACCUGCGCACTT (antisense), GGGUUUUCGCGGU UCACAUTT (sense), AUGUGAACCACGAAAACCCTT (antisense), GGGUU UUCGUGGUUCACAUTT (sense), and AUGUGAACCACCACGAAAAC CCTT (antisense), for p53, GGAAACUACUUCCUGAAAATT (sense), UUUU CAGGAAGUAGUUUCCTT (antisense), CUGGAAGACUCCAGUGGUATT (sense), UACCACUGGAGUCUUCCAGTT (antisense), CUUAGUACCUAAA AGGAAATT (sense), and UUUCCUUUUAGGUACUAAGTT (antisense). Transfected cells were incubated with or without TAM, and confocal or flow cytometric analysis was performed.

Western blotting. Whole-cell extracts of HSG or RH0 cells were purified using radioimmunoprecipitation assay buffer (50 mM Tris-HCl, pH 7.4, 150 mM NaCl, 1 mM EDTA, 1% NP-40, 1 mM dithiothreitol [DTT], 1 mM phenylmethylsulfonyl fluoride) supplemented with a protease inhibitor cocktail (Sigma Chemical Co., St. Louis, MO). After centrifugation for 20 min at 12,000 rpm at 4°C, the supernatant was extracted and used for samples. Also, to detect α-fodrin in organs, tissue samples from OVX and sham C57BL/6 mice were extracted as described above. Ten micrograms of each sample per well was used for 7.5 to 12.5% sodium dodecyl sulfate-polyacrylamide gel electrophoresis and transferred to polyvinylidene difluoride membranes, which were probed with anti-RbAp48, anti-Rb (p110 and p130), anti-Bad, anti-Bax, anti-ARF (p14 and p19), anti-cyclin D3 (BD Transduction Laboratories, Lexington, KY), anti-Mdm2, anti-E2F-1, anti-phospho-Rb (Sigma), anti-p53, anti-phospho-p53 Ab sampler kit (Ser6, Ser9, Ser15, Ser20, Ser37, Ser46, and Ser392; Cell Signaling Technology Inc., Beverly, MA), anti-α-fodrin (Affiniti, Mamhead, United Kingdom), and anti-p21 (Santa Cruz Biotechnology, Santa Cruz, CA) as the primary Abs, and anti-α-tubulin, GAPDH, or histone MAb (Sigma) as internal control. The nitrocellulose membranes were incubated with peroxidase-conjugated horse anti-mouse or rabbit immunoglobulin G (IgG; Vector Laboratories) as the secondary Ab. Protein binding was visualized with ECL Western blotting reagent (Amersham Corp., Arlington Heights, IL).

TUNEL assay. Apoptotic cells were detected in sections using the in situ terminal deoxynucleotidyltransferase (TdT)-mediated dUTP-biotin nick end labeling (TUNEL) kit (Wako). Sections were incubated with proteinase K (20 μg/ml) for 10 min and then presoaked in TdT buffer (0.5 μM cacodylate, 1 mM CoCl, 0.5 μM DTT, 0.05% bovine serum albumin, 0.15 M NaCl) for 10 min. Sections were incubated for 2 h at 37°C in 25 μl of TdT solution, containing 1× terminal transferase buffer, 0.5 nmol of biotin-dUTP, and 10 U of TdT. After the TdT reaction, sections were soaked in TdT blocking buffer (300 nM NaCl, 30 mM Tris-sodium citrate-2-hydrate), incubated with horseradish peroxidase-conjugated streptavidin for 30 min at room temperature, and developed for 10 min in phosphate-buffered citrate (pH 5.8) containing 0.6 mg/ml DAB (3,3′-diaminobenzidine-tetrahydrochloride-dihydrate). Nuclei were counterstained with hematoxylin. For confocal microscopic analysis, FITC-labeled UTP was used.

Caspase activity assay. Caspase activities were assayed using a caspase family colorimetric substrate set (BioVision Inc.). Briefly, 100 μg of cytoplasmic lysates of RH0 cells was incubated with 200 μM Ac-YVAD-pNA (caspase 1 substrate), Ac-VDVAD-pNA (caspase 2 substrate), Ac-DEVD-pNA (caspase 3 substrate), Ac-WEHD-pNA (caspase 5 substrate), Ac-VEID-pNA (caspase 6 substrate), Ac-IETD-pNA (caspase 8 substrate), and Ac-LEHD-pNA (caspase 9 substrate) at 37°C for 1 h. The absorbance of samples was read at 405 nm in a microtiter plate reader. The relative percent increase in caspase activity was determined by comparing these results with the level of the uninduced control.

Gel shift assay. Nuclear extracts were prepared from RH0 cells by a method previously described (29). Nuclear extracts containing 5 μg of protein were incubated in 20 μl of binding buffer (10 mM Tris-HCl, pH 8.0, 50 mM NaCl, 1 mM MgCl2, 0.5 mM DTT, and 4% glycerol) with or without a cold competitor. The E2F-1 DNA probe, 5′-TCCGTAGTTTTCGCGCTTAAATTTGAGAAAG GGCGCGAAACTAGTC-3′ (10,000 cpm) labeled with [γ-^{32}P]ATP was added, and the samples were incubated at room temperature for 20 min. Reaction mixtures were separated in a 4% polyacrylamide gel and autoradiographed on X-ray film (Fujifilm, Kanagawa, Japan).

Immunohistochemical analysis. Immunohistochemical analysis of RbAp48 expression was performed on the sections of salivary and lacrimal glands from sham, OVX B6, RbAp48-WT (wild type), and RbAp48-TG mice. Paraffin-embedded sections were stained with anti-RbAp48 MAb (BD Transduction Laboratories) as the primary Ab. Protein binding was detected with an LSAB2 kit containing horseradish peroxidase (DAKO, Carpineteria, CA) and DAB as a substrate. The counterstaining of nuclei was performed with hematoxylin.

Confocal microscopy. Confocal microscopic analysis of RbAp48, E2F-1, ARF, and p53 expression, and TUNEL-positive cells was performed on the cultured cells, and frozen sections of salivary glands from sham, OVX $ER\alpha^{-/-}$, $p53^{-/-}$,

MSG cells from B6 mice, and the inhibitory effects with siRNA of RbAp48 construct were observed by confocal microscopic analysis. The percentage of $TUNEL^+$ apoptotic cells was enumerated as described. Cont, irrelevant siRNA control. Images are representative of three independent experiments. (D) TAM-induced apoptosis was not associated with RbAp48 expression in the primary culture of MMG cells from B6 mice. $TUNEL^+$ apoptotic cells were enumerated as described. Images are representative of three independent experiments.

E2F1$^{-/-}$, RbAp48-WT, and RbAp48-TG mice using a Confocal Laser Microscan (LSM 5 PASCAL; Carl Zeiss, Germany). As the second Abs, Alexa Fluor 488–anti-mouse IgG heavy and light chain [IgG (H+L)], Alexa Fluor 568–goat anti-rabbit IgG (H+L), Alexa Fluor 488–donkey anti-rat IgG (H+L), Alexa Fluor 488–chicken anti-goat IgG (H+L), and Alexa Fluor 568–rabbit anti-goat IgG (H+L) were used. Nuclear DNA was stained with 4′,6-diamidino-2-phenylindole dihydrochloride.

BrdU incorporation. MSG cells from RBAp48 TG and WT mice were stimulated with phorbol 12-myristate 13-acetate for 24 h, and 10 mM bromodeoxyuridine (BrdU) was incorporated for the last 2 h. Fixed and permeabilized cells were treated with DNase and stained with FITC-conjugated anti-BrdU antibody (BD Pharmingen, San Diego, CA). The polyvinylidene difluoride DNA synthetic activity was analyzed by flow cytometry.

RESULTS

Identification of TAM-induced gene. We found a time-dependent increase in apoptotic HSG cells stimulated with TAM, and E2 treatment inhibited the apoptosis (Fig. 1A). To identify gene products specific to TAM-induced apoptosis in the salivary gland cells, mRNAs from HSG cells treated with TAM and nontreated cells were analyzed by a differential display PCR method. From the samples isolated with the highest grade of differential expression, we analyzed the mRNAs from HSG cells treated with TAM and nontreated cells by a reverse Northern blotting technique (Fig. 1B). The sequence of TAM-induced mRNA corresponds (100%) to RbAp48. The expression of RbAp48 mRNA in HSG cells reached peak level at 2 h after stimulation with TAM, and then the level decreased, whereas increased expression of RbAp48 mRNA in MCF-7 cells was not observed (Fig. 1C). We confirmed the inhibitory effects of siRNA on TAM-induced apoptosis in HSG cells, not MCF-7 cells, with siRNA (5 to 50 nM) of RbAp48 construct (Fig. 1D). In addition, a dose-dependent inhibition of siRNA (0 to 200 nM) on TAM-induced RbAp48 expression in HSG cells, not MCF-7 cells, was observed (Fig. 1E). We next searched the tissue distribution of RbAp48 mRNA using human tissue total RNA-blotted membrane by Northern blot analysis. We found the highest level of expression of RbAp48 mRNA in the testis, which is consistent with the previous report (33), and the lowest was found in the parotid salivary gland (Fig. 1F), although the molecular mechanism by which the lowest RbAp48 mRNA is expressed in the parotid glands is unclear.

RbAp48 overexpression in estrogen-deficient mice. To confirm the in vivo overexpression of RbAp48 and apoptosis in estrogen-deficient B6 mice, OVX was performed on mice at the age of 4 weeks. Using Western blotting, we detected a time-dependent increase in RbAp48 in the salivary and lacrimal gland tissues from 0 to 3 weeks after OVX (at the age of 4 to 7 weeks) but not in other organs, including mammary glands (Fig. 2A). RbAp48^{+} and TUNEL^{+} apoptotic cells were detected by immunohistochemical analysis in the salivary and lacrimal gland sections from OVX B6 mice at the age of 7 weeks but not in sham mice (Fig. 2B). In vitro studies using primary cultured cells from B6 mice demonstrated that TAM-induced apoptosis was associated with RbAp48 expression in MSG cells but not in MMG cells (Fig. 2C and D). We confirmed the inhibitory effects of siRNA in MSG cells but not in MMG cells with siRNA of RbAp48 construct (Fig. 2C and D).

RbAp48 as a novel apoptosis-inducible gene. RbAp48 mRNA expression and apoptosis could be induced in HSG cells stimulated with TAM and a pure antiestrogen, ICI182780, but not with other apoptotic stimuli such as staurosporin, paclitaxel, anti-Fas MAb, and etoposide (Fig. 3A). This indicates that induction of RbAp48 mRNA expression might be dependent on estrogen deficiency. To ensure the role of RbAp48 in various types of cells, RbAp48 was transiently transfected, and apoptosis was determined by flow cytometry using an annexin V-FITC apoptosis detection kit. Among the cells examined (HSG, MSG, MCF-7, HT-29, Colo201, HeLa, HepG2, SH-SY5Y, NEC14, THP-1, Jurkat, Raji, U937, and WI38), significant apoptosis was induced exclusively in the salivary gland cells transfected with RbAp48 of both human and mouse origin (Fig. 3B). Notably, apoptosis was induced by transfection with RbAp48 cDNA in MSG cells isolated from ER$\alpha^{-/-}$ mice, indicating that this signaling might act in the downstream of estrogen-ER binding. Apoptotic cells could not be induced by the transgene of RbAp48 cDNA but was induced by TAM in MCF-7 cells. We confirmed that the induction levels of RbAp48 are the same in the other cell lines including Jurkat and THP-1 as the HSG cells (Fig. 3C). We next generated and analyzed the RbAp48-stable cell line (RH0), which was an IPTG-inducible transfectant of RbAp48 in HSG cells, with a LacSwitch II Inducible Mammalian Expression System using repressor and operator vectors. Apoptosis was drastically induced in IPTG-treated RH0 cells in association with RbAp48 expression within 8 h (Fig. 3D). When we examined the effect of siRNA on RbAp48-induced apoptosis, the apoptosis in IPTG-treated RH0 cells was clearly inhibited by siRNA of RbAp48 but not by siRNA of GAPDH or an irrelevant control (Fig. 3E).

Molecular mechanisms for RbAp48-induced apoptosis. We next examined the molecular mechanisms responsible for RbAp48-induced apoptosis. We detected upregulation of phosphorylated Rb, cyclin D3, p14ARF, Bax, Bad, cytochrome *c* (Cyt *c*) and a cleavage product of α-fodrin (arrow) in IPTG-treated RH0 cells (Fig. 4A). Our previous report demonstrated that α-fodrin is a candidate autoantigen of primary Sjögren's syndrome (10). When nuclear extracts of IPTG-treated RH0 cells were analyzed by gel shift assay, DNA binding activity of E2F-1 was detected in RbAp48-induced apoptotic cells (Fig. 4B). E2F-1 protein was also detected in the nuclear extract by Western blotting (Fig. 4B). It has been proposed that the E2F-1 transcription factor serves as a link between the Rb/E2F proliferation pathway and the p53 apoptosis pathway by inducing the expression of p14ARF, a protein that regulates p53 stability (36). We next focused on the p53-dependent pathway, because MSG cells transfected with RbAp48 isolated from p53$^{-/-}$ mice are apoptosis resistant (Fig. 4C). When Adp53-infected MSG cells were transfected with the RbAp48 gene, apoptosis was rapidly induced (Fig. 4C). Phosphorylated p53 (Ser9) was found by Western blotting after 2 to 4 h, but no other phosphorylated p53 (Ser15, Ser20, and Ser392) was detected (Fig. 4D). The phosphorylation of p53 in the other sites (Ser6, Ser37, and Ser46) was not observed (data not shown). We also confirmed a time-dependent downregulation of Mdm2 (Fig. 4D), which is important as a regulatory partner of p53 (47). Using Western blotting, we also detected increased p21 expression, a major player in the p53-mediated pathway, in IPTG-treated RH0 cells (Fig. 4E). p53 induces apoptosis by a multitude of molecular pathways, in addition to transactivation

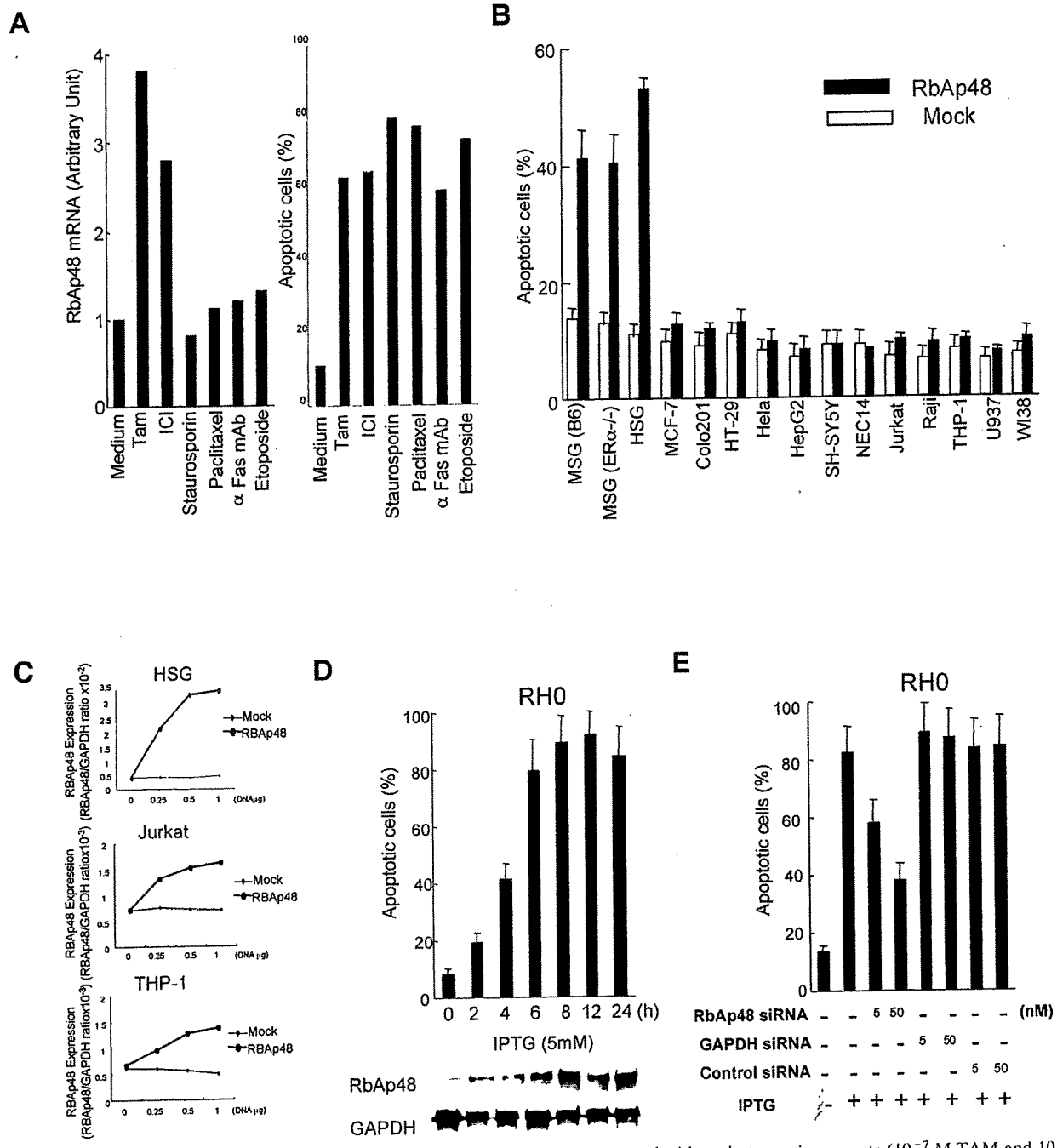

FIG. 3. Role of RbAp48 in salivary gland cell apoptosis. (A) HSG cells were treated with antiestrogenic reagents (10^{-7} M TAM and 10^{-7} M ICI182780) and general apoptotic stimuli (staurosporin, paclitaxel, anti-Fas MAb, and etoposide). RbAp48 mRNA was quantitated with BAS-2000II, and message level was expressed as the ratio of RbAp48 mRNA/β-actin mRNA; the percentage of apoptotic cells was detected by FITC-annexin V-PI was expressed for all of these agents. Graphs are representative of three independent experiments. (B) The RbAp48 gene was transiently transfected into various cells using FuGENE6. At 48 h after transfection of pCMV-RbAp48 plasmid or pCMV (mock) plasmid, apoptotic cells were detected by FITC-annexin V-PI. Data are the means ± standard deviations of triplicate samples. The graph is representative of three independent experiments. (C) The levels of the induction ratio of RbAp48 were shown to be the same in the other cell lines including Jurkat and THP-1 as the HSG cells using Western blot analysis. The levels were expressed as the ratio of RbAp48/GAPDH protein. (D) Establishment of the RbAp48 stable cell clone. An increase in RbAp48 expression and apoptosis of IPTG-treated RH0 cells were observed in a time-dependent manner. Apoptotic cells were detected by FITC-annexin V-PI. Data are means ± standard deviations of triplicate samples. Expressions of RbAp48 and GAPDH as an internal control were detected by Western blot analysis. Graph and images are representative of four independent experiments. (E) Inhibitory effects of siRNA on RbAp48-induced apoptosis. IPTG-treated RH0 cells were cotransfected with siRNA (5 to 50 nM) of RbAp48 and pCMV-GFP. Apoptotic cells gated on GFP^+ were detected by PE-conjugated annexin V. Data are means ± standard deviations of triplicate samples. Graph is representative of three independent experiments.

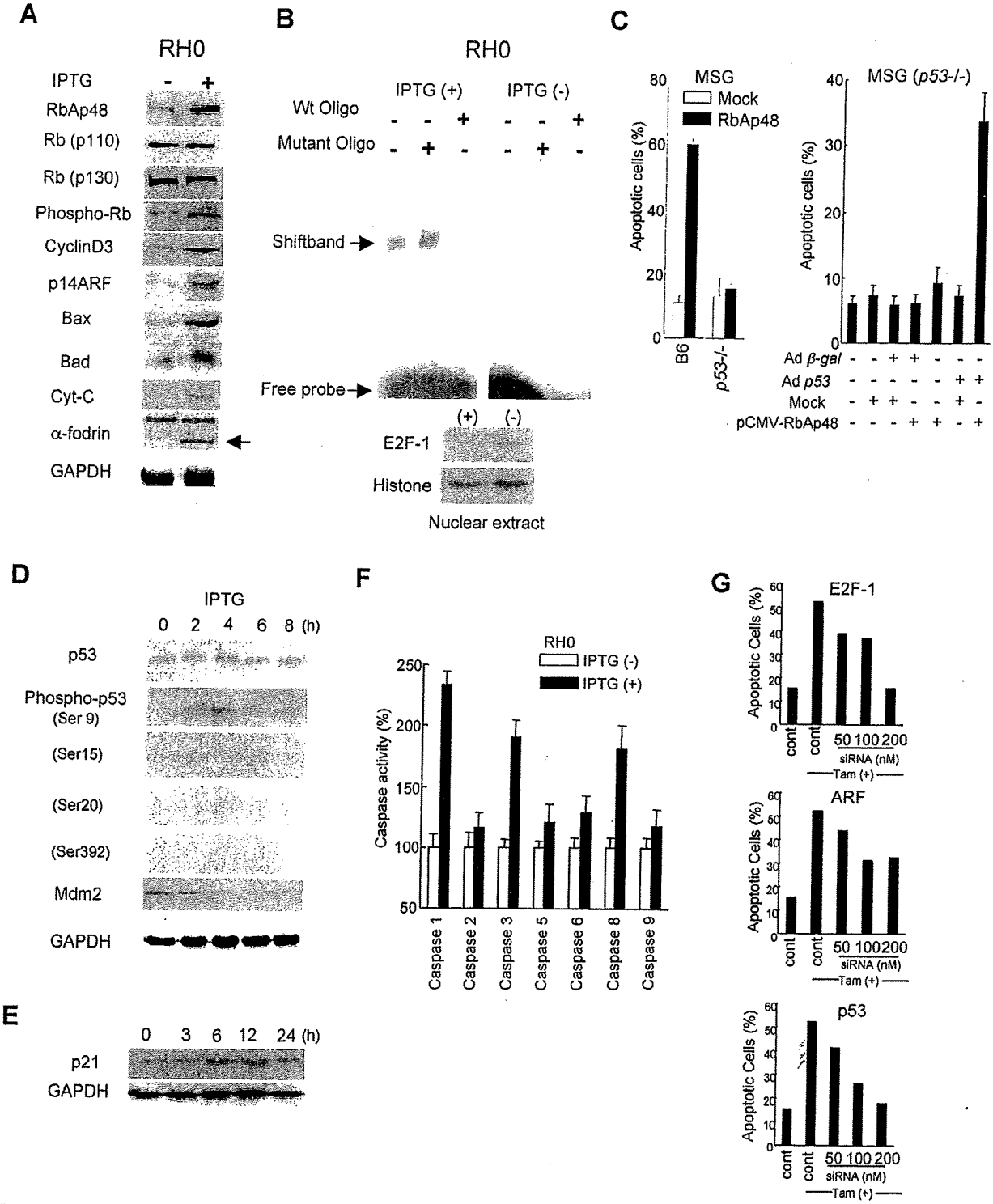

FIG. 4. Molecular mechanisms responsible for RbAp48-induced apoptosis. (A) Contribution of cell cycle and mitochondrion-related molecules in RbAp48-induced apoptosis of RH0 cells. The lysates of IPTG-treated or nontreated RH0 cells were used to detect RbAp48, Rb (p110 and p130), phospho-Rb, cyclin D3, p14ARF, Bax, Bad, Cyt-*c*, the cleavage product of α-fodrin, and GAPDH for Western blot analysis. Blots are representative of three independent experiments. (B) Detection of E2F-1 transcriptional activity in RbAp48-induced apoptosis. The nuclear proteins of IPTG-treated RH0 cells were analyzed by gel shift assay with an E2F-1 binding DNA probe. To confirm the specific binding to the E2F-1 binding site, the mutant oligonucleotide and wild-type oligonucleotide as a competitor were used for this assay. E2F-1 protein was detected in the nuclear extract by Western blotting. Histone was used for an internal control. Blots are representative of three independent experiments. (C) Apoptosis of MSG cells from $p53^{-/-}$ mice was not observed by RbAp48 gene transfection. Transfection with pCMV (Mock) was used as control. MSG ($p53^{-/-}$) cells were infected with Ad*p53* and incubated for 24 h. The infected cells were cotransfected with the RbAp48 gene and

of target genes, and it can elicit apoptosis by transcription-independent mechanisms (5, 28). Although apoptosis in response to p53 activation is often accompanied by caspase activation, the mechanisms underlying p53-induced caspase activation remain poorly understood. Caspase activities in RbAp48-induced apoptosis in HSG cells were assayed using a caspase family colorimetric substrate set. A significant increase in caspase 1 activity was detected with relatively elevated caspase 3 and 8 activity on RbAp48-induced apoptotic HSG cells (Fig. 4F). RbAp48-induced apoptosis in HSG cells was clearly inhibited by siRNA of E2F-1 and p53 but only moderately by siRNA of ARF (Fig. 4G).

RbAp48/E2F1/ARF-p53 pathway in the salivary glands. We evaluated the effects of RbAp48 overexpression and knockdown in primary MSG cells and documented the effects on E2F-1, ARF, and p53 protein levels in these cells. We demonstrated that overexpression of RbAp48 in MSG cells from B6 mice induced E2F-1, p19ARF, and phospho-p53 expression, and the inhibitory effect of siRNA of RbAp48 was observed from confocal microscopic analysis (Fig. 5A). We next examined whether TAM-induced apoptosis is associated with RbAp48 expression in MSG cells from B6 mice, compared with cells from $ER^{-/-}$, $E2F1^{-/-}$, and $p53^{-/-}$ mice. By confocal microscopic analysis, we found that TAM-induced apoptosis was associated with RbAp48 expression in MSG cells from B6 mice but not from $ER^{-/-}$, $E2F1^{-/-}$, and $p53^{-/-}$ mice Fig. (5B). We further examined the effect of OVX on the expression of RbAp48, E2F-1, p19ARF, and phospho-p53 in MSG cells from B6, $ER^{-/-}$, $E2F1^{-/-}$, and $p53^{-/-}$ mice. By double-labeled confocal microscopy, we found coexpression of RbAp48/E2F1, RbAp48/p19ARF, and RbAp48/p53 in MSG cells from OVX B6 mice but not from B6 mice (Fig. 5C). No differences in RbAp48/E2F1, RbAp48/p19ARF, and RbAp48/phospho-p53 expression levels were observed in MSG cells from non-OVX and OVX $ER^{-/-}$, $E2F1^{-/-}$, and $p53^{-/-}$ mice (Fig. 5C).

Findings in RbAp48-transgenic mice. We constructed several lines of B6 background TG mice (39) expressing RbAp48 in the salivary glands using Lama promoter as described in Materials and Methods. Prominent expression of RbAp48 in the salivary glands from TG mice was determined at the age of 8 to 20 weeks by both immunohistochemistry and Western blotting (Fig. 6A and B). No difference in RbAp48 expression in the spleen was observed between TG and WT mice. A considerable number of $TUNEL^+$ apoptotic epithelial duct cells were found in the salivary glands of RbAp48-TG mice but not WT mice at the age of 20 weeks (Fig. 6C). In addition, expression of E2F-1, p19ARF, and phospho-p53 was observed in the salivary glands of RbAp48-TG mice but not WT mice (Fig. 6D). BrdU studies of TG mice with ectopic RbAp48 in the salivary glands demonstrated that cellular proliferation is barely affected (Fig. 6E). No pathological findings were observed in other organs of TG mice.

DISCUSSION

In this study, we demonstrated the first evidence that gender-based, tissue-specific apoptosis could be induced in the exocrine gland cells through RbAp48 overexpression with p53 phosphorylation. Indeed, RbAp48 overexpression with apoptosis was observed in the exocrine glands in OVX C57BL/6 mice, and transgenic expression of the RbAp48 gene induced tissue-specific apoptosis in the exocrine glands.

RbAp48, initially identified as a retinoblastoma binding protein (34), was characterized as a component of distinct nucleosome-modifying complexes, including the nuclear histone deacetylases (18, 25). In general, the functions of the RbAp48-like proteins in these complexes remain undetermined. It was reported that E2F-1 and RbAp48 are physically associated in the presence of Rb and histone deacetylase (26), suggesting that RbAp48 could be involved in transcriptional repression of E2F-responsive genes. The induction of apoptosis in various cell lines is accompanied by a shift in Rb from the hyper- to the hypophosphorylated form (49). Rb dephosphorylation, which has been shown to be required for apoptosis, occurs in the early stage of apoptosis (6). Loss of Rb function can induce p53-dependent apoptosis, but little is known about the mechanisms of Rb-regulated p53-dependent apoptosis. Recently, Lieman et al. provided evidence for a novel mechanism linking Rb-E2F to the extrinsic apoptotic pathway through inactivation of focal adhesion kinase and activation of caspase 8 (20). It has been proposed that the E2F-1 transcription factor serves as a link between the Rb/E2F proliferation pathway and the p53 apoptosis pathway by inducing the expression of p14ARF, a protein that regulates p53 stability. Recent observations have revealed that p53 can directly translocate to mitochondria and induce apoptosis in a transactivation-independent manner (21). In this study, we confirmed a time-dependent downregulation of Mdm2, which is important as a regulatory partner of p53 (47). In addition to regulation of p53, Mdm2 has been reported to stimulate E2F-1 transactivation by a mechanism that remains unclear. E2F-1 can signal p53 phosphorylation in the absence of p14ARF, similar to the observed modifications to p53 in response to DNA damage. p53 modification is found to be crucial for E2F-1-mediated apoptosis, and this apoptosis is compromised when E2F-1 is coexpressed with a p53 mutant

pCMV-GFP, and then apoptosis was detected by PE-annexin V on GFP^+ cells. Infection of adenovirus β-galactosidase was used as a control. Graphs are representative of five independent experiments. (D) Expression levels of p53, phospho-p53 (Ser9), and Mdm2 in IPTG-treated RH0 cells. Other phosphorylated p53 proteins (Ser15, Ser20, and Ser392) were not detected. GAPDH expression was used for an internal control. Blots are representative of three independent experiments. (E) Detection of increased p21 expression, a major player in the p53-mediated pathway, by Western blotting. Blot is representative of two independent experiments. (F) Caspase activities of IPTG-treated RH0 cells were analyzed by a caspase enzymatic activity assay. A significant increase in caspase-1 activity was detected with relatively elevated caspase 3 and 8 activity. The absorbance of samples was read at 405 nm in a microtiter plate reader and the relative percent increase in activity was calculated by comparing the absorbance of IPTG-treated cells with that of untreated cells. Data are means ± standard deviations of triplicate samples. The graph is representative of three independent experiments. (G) RbAp48-induced apoptosis in HSG cells was clearly inhibited by siRNAs of E2F-1 and p53 but only moderately by siRNA of ARF. Graphs are representative of three independent experiments.

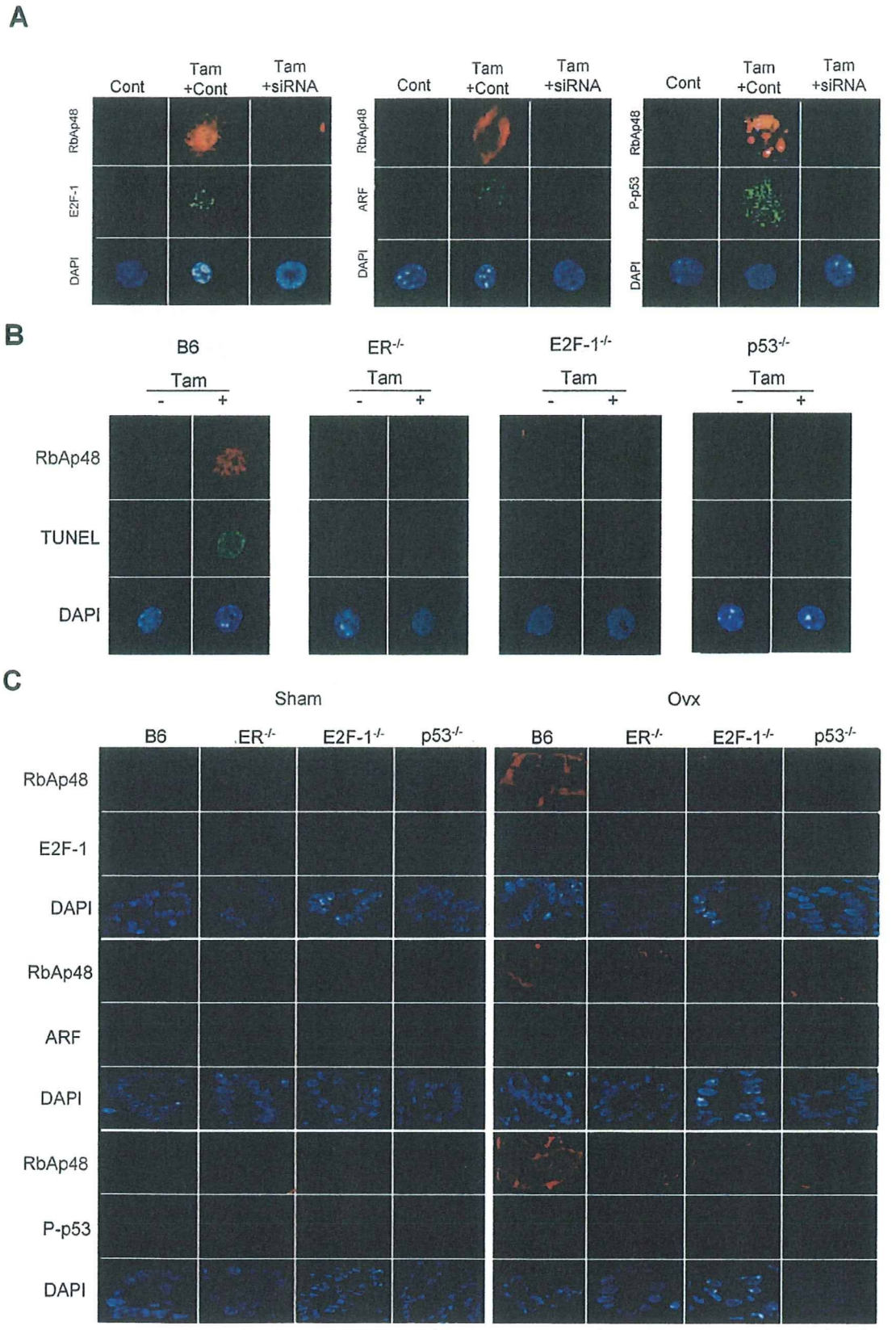
A
Cont
Tam +Cont
Tam +siRNA
RbAp48
E2F-1
DAPI
Cont
Tam +Cont
Tam +siRNA
RbAp48
ARF
DAPI
Cont
Tam +Cont
Tam +siRNA
RbAp48
P-p53
DAPI
B
B6
ER-/-
E2F-1-/-
p53-/-
Tam
- +
RbAp48
TUNEL
DAPI
C
Sham
Ovx
B6
ER-/-
E2F-1-/-
p53-/-
RbAp48
E2F-1
DAPI
RbAp48
ARF
DAPI
RbAp48
P-p53
DAPI

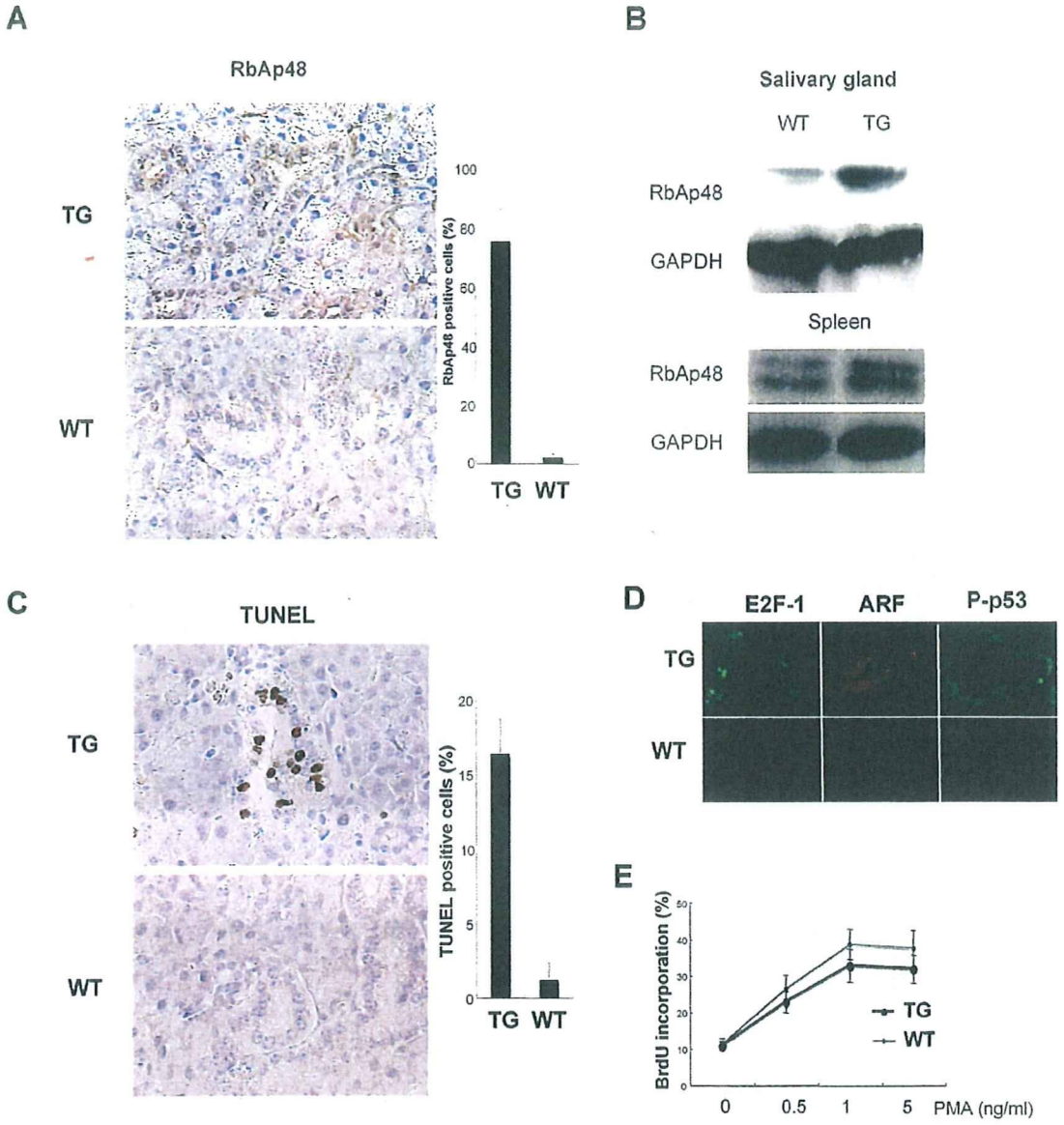

FIG. 6. RbAp48 overexpression and apoptosis in TG mice. (A) RbAp48 overexpression in the salivary gland tissues of TG mice but not WT mice at the age of 20 weeks detected by immunohistology. The percentage of RbAp48$^+$ cells was enumerated as described above (legend of Fig. 2B). (B) RbAp48 expression in the salivary gland tissues at the age of 20 weeks of TG mice compared with age-matched WT mice as detected by Western blotting. No differences in the levels of RbAp48 expression in spleens of WT and TG mice were detected. GAPDH expression was used for an internal control. (C) TUNEL$^+$ apoptotic epithelial duct cells were found in salivary glands of TG mice but not of age-matched WT mice at the age of 20 weeks. The percentage of TUNEL$^+$ cells was enumerated as described above. Images are representative of five mice. (D) Expression of E2F-1, p19ARF, and P-p53 was observed by confocal microscopy in the salivary glands of RbAp48-TG mice but not WT mice. Images are representative of five mice. (E) BrdU studies of TG mice with ectopic RbAp48 in the salivary glands demonstrated that cellular proliferation is barely affected. The graph is representative of three mice.

FIG. 5. RbAp48/E2F1/ARF-p53 pathway in the salivary glands. (A) Overexpression of RbAp48 in MSG cells from B6 mice induced E2F-1, p19ARF, and phospho-p53 (P-p53) expression, and the inhibitory effect of siRNA (15 nM) of RbAp48 was observed by confocal microscopic analysis. Cont, irrelevant siRNA control. Images are representative of three independent experiments. (B) TAM-induced apoptosis was associated with RbAp48 in MSG cells from B6 mice but not from ER$^{-/-}$, E2F1$^{-/-}$, and p53$^{-/-}$ mice as detected by confocal microscopy. Images are representative of two independent experiments. (C) Coexpression of RbAp48/E2F1, RbAp48/p19ARF, and RbAp48/p53 was detected by double-labeled confocal microscopic analysis in MSG cells of OVX B6 mice but not sham B6 mice. No differences in RbAp48/E2F1, RbAp48/p19ARF, and RbAp48/p53 expression levels were observed in MSG cells of non-OVX and OVX ER$^{-/-}$, E2F1$^{-/-}$, and p53$^{-/-}$ mice. Photos are representative of two independent experiments.

lacking many N- and C-terminal phosphorylation sites (36). These findings suggest that p53 phosphorylation is a key step in E2F-1-mediated apoptosis. The transcription factor E2F-1 functions as a key regulator for both cell cycle progression and apoptosis. E2F-2-deficient T lymphocytes exhibit enhanced T-cell receptor-stimulated proliferation and a lower activation threshold, leading to the accumulation of a population of autoreactive T lymphocytes, which appear to be responsible for causing autoimmunity in E2F-2-deficient mice (24). E2F-1$^{-/-}$ mice exhibit a defect in T lymphocyte development leading to an excess of mature T cells due to a maturation stage-specific defect in thymocyte apoptosis (8).

Our recent study suggests that antiestrogenic actions have a potent effect on the proteolysis of α-fodrin autoantigen in the salivary glands through upregulation of caspase 1 and caspase 3 activity (14). We found here a proteolysis of α-fodrin and a significant increase in caspase 3 activity in addition to the elevated caspase 1 and caspase 8 activity on RbAp48-induced apoptotic HSG cells. The fodrin α-subunit of various cells has been shown to be cleaved in association with apoptosis, in particular, due to upregulation of caspase 3 (4, 15, 48). Several reports have demonstrated that estrogen may play an inhibitory role in apoptosis in endothelial cells, breast cancer cells, cardiac myocytes, prostate cells, and neuronal cells (30, 32, 41, 43). Moreover, it has been noted that some enzymatic activities are elevated in postmenopausal women compared with normal healthy women (1, 27). Increased caspase levels seem to potentiate cell death in the presence of p53-generated signals that trigger caspase activation. Activated caspases digest many cellular proteins responsible for cell cycle regulation (e.g., Rb and Mdm2) (16), DNA damage recognition and repair [e.g., DNA-dependent protein kinase, p53, and poly(ADP-ribose) polymerase], and regulation of the cellular structure (e.g., actin, lamin, and fodrin) (44, 45). All these functional and structural protein modifications lead directly to apoptosis. Moreover, RbAp48 is found not only in histone deacetylase complexes but also in ATP-dependent remodeling complexes (9). Here we show that RbAp48 specifically activates E2F-1-mediated p53 phosphorylation in the salivary gland cells but not in many of the other types of cells examined. Thus, although the association of RbAp48 with nuclear transcriptional coactivators has not been described, there is abundant evidence that these histone binding factors interact with related classes of proteins (53, 46).

Taken together, our results demonstrate a direct molecular mechanism by which estrogen deficiency might promote p53-mediated apoptosis exclusively in exocrine gland cells through RbAp48 overexpression.

ACKNOWLEDGMENT

This work was supported in part by a Grant-in-Aid for Scientific Research (no. 17109016 and 17689049) from the Ministry of Education, Science and Culture of Japan.

REFERENCES

1. **Acarturk, F., and J. R. Robinson.** 1996. Vaginal permeability and enzymatic activity studies in normal and ovariectomized rabbits. Pharm. Res. **13**:779–783.
2. **Apostolou, I., Z. Hao, K. Rajewsky, and H. von Boehmer.** 2003. Effective destruction of Fas-deficient insulin-producing B cells in type 1 diabetes. J. Exp. Med. **198**:1103–1106.
3. **Christen, U., and M. G. Von Herrath.** 2002. Apoptosis of autoreactive CD8 lymphocytes as a potential mechanism for the abrogation of type 1 diabetes by islet-specific TNF-α expression at a time when the autoimmune process is already ongoing. Ann. N. Y. Acad. Sci. **958**:166–169.
4. **Cryns, V. L., L. Bergeron, H. Zhu, H. Li, and J. Yuan.** 1996. Specific cleavage of alpha-fodrin during Fas- and tumor necrosis factor-induced apoptosis is mediated by an interleukin-1beta-converting enzyme/Ced-3 protease distinct from the poly(ADP-ribose) polymerase protease. J. Biol. Chem. **271**:31277–31282.
5. **Ding, H. F., Y. L. Lin, G. McGill, P. Juo, H. Zhu, J. Blenis, J. Yuan, and D. E. Fisher.** 2000. Essential role for caspase-8 in transcription-independent apoptosis triggered by p53. J. Biol. Chem. **275**:38905–38911.
6. **Dou, Q. P., B. An, and P. L. Will.** 1995. Induction of a retinoblastoma phosphatase activity by anticancer drugs accompanies p53-independent G1 arrest and apoptosis. Proc. Natl. Acad. Sci. USA **92**:9019–9023.
7. **Enders, A., P. Bouillet, H. Puthalakath, Y. Xu, D. M. Tarlinton, and A. Strasser.** 2003. Loss of the proapoptotic BH3-only Bcl-2 family member Bim inhibits BCR stimulation-induced apoptosis and deletion of autoreactive B cells. J. Exp. Med. **198**:1119–1126.
8. **Field, S. J., F. Y. Tsai, F. Kuo, A. M. Zubiaga, W. G. Kaelin, Jr., D. M. Livingston, S. H. Orkin, and M. E. Greenberg.** 1996. E2F-1 functions in mice to promote apoptosis and suppress proliferation. Cell **85**:549–561.
9. **Gdula, D. A., R. Sandaltzopoulos, T. Tsukiyama, V. Ossipow, and C. Wu.** 1998. Inorganic pyrophosphatase is a component of the *Drosophila* nucleosome remodeling factor complex. Genes Dev. **12**:3206–3216.
10. **Haneji, N., T. Nakamura, K. Takio, K. Yanagi, H. Higashiyama, I. Saito, S. Noji, H. Sugino, and Y. Hayashi.** 1997. Identification of α-fodrin as a candidate autoantigen in primary Sjogren's syndrome. Science **276**:604–607.
11. **Hiebert, S. W.** 1993. Regions of the retinoblastoma gene product required for its interaction with the E2F transcription factor are necessary for E2 promoter repression and pRb-mediated growth suppression. Mol. Cell. Biol. **13**:3384–3391.
12. **Hugues, S, E. Mougneau, W. Ferlin, D. Jeske, P. Hofman, D. Homann, L. Beaudoin, C. Schrike, M. Von Herrath, A. Lehuen, and N. Glaichenhaus.** 2002. Tolerance to islet antigens and prevention from diabetes induced by limited apoptosis of pancreatic β cells. Immunity **16**:169–181.
13. **Ishimaru, N., K. Saegusa, K. Yanagi, N. Haneji, I. Saito, and Y. Hayashi.** 1999. Estrogen deficiency accelerates autoimmune exocrinopathy in murine Sjogren's syndrome through Fas-mediated apoptosis. Am. J. Pathol. **155**:173–181.
14. **Ishimaru, N., R. Arakaki, M. Watanabe, M. Kobayashi, K. Miyazaki, and Y. Hayashi.** 2003. Development of autoimmune exocrinopathy resembling Sjogren's syndrome in estrogen deficient mice of healthy background. Am. J. Pathol. **163**:1481–1490.
15. **Janicke, R. U., M. L. Sprengart, M. R. Wati, and A. G. Porter.** 1998. Caspase-3 is required for DNA fragmentation and morphological changes associated with apoptosis. J. Biol. Chem. **273**:9357–9360.
16. **Katsuda, K., M. Kataoka, F. Uno, T. Murakami, T. Kondo, J. A. Roth, N. Tanaka, and T. Fujiwara.** 2002. Activation of caspase-3 and cleavage of Rb are associated with p16-mediated apoptosis in human non-small cell lung cancer cells. Oncogene **21**:2108–2113.
17. **Kyprianou, N., H. F. English, N. E. Davidson, and J. T. Isaacs.** 1991. Programmed cell death during regression of the MCF-7 human breast cancer following estrogen ablation. Cancer Res. **51**:162–166.
18. **Lai, A., J. M. Lee, W. M. Yang, J. A. DeCaprio, W. G. Kaelin, Jr., E. Seto, and P. E. Branton.** 1999. RBP1 recruits both histone deacetylase-dependent and -independent repression activities to retinoblastoma family proteins. Mol. Cell. Biol. **19**:6632–6641.
19. **Lamhamedi-Cherradi, S. E., S. J. Zheng, K. A. Maguschak, J. Peschon, and Y. H. Chen.** 2003. Defective thymocyte apoptosis and accelerated autoimmune diseases in TRAIL$^{-/-}$ mice. Nat. Immunol. **4**:255–260.
20. **Lieman, J. H., L. A. Worley, and J. W. Harbour.** 2005. Loss of Rb-E2F repression results in caspase-8-mediated apoptosis through inactivation of focal adhesion kinase. J. Biol. Chem. **280**:10484–10490.
21. **Marchenko, N. D., A. Zaika, and U. M. Moll.** 2000. Death signal-induced localization of p53 protein to mitochondria. A potential role in apoptotic signaling. J. Biol. Chem. **275**:16202–16212.
22. **Mikkelsen, T. R., J. Brandt, H. J. Larsen, B. B. Larsen, K. Poulsen, J. Ingerslev, N. Din, and J. P. Hjorth.** 1992. Tissue-specific expression in the salivary glands of transgenic mice. Nucleic Acids Res. **20**:2249–2255.
23. **Miyagishi, M., and K. Taira.** 2002. U6 promoter-driven siRNAs with four uridine 3′ overhangs efficiently suppress targeted gene expression in mammalian cells. Nat. Biotechnol. **20**:497–500.
24. **Murga, M., O. Fernandez-Capetillo, S. J. Field, B. Moreno, L. R. Borlado, Y. Fujiwara, D. Balomenos, A. Vicario, A. C. Carrera, S. H. Orkin, M. E. Greenberg, and A. M. Zubiaga.** 2001. Mutation of E2F2 in mice causes enhanced T lymphocyte proliferation, leading to the development of autoimmunity. Immunity **15**:959–970.
25. **Nicolas, E., S. Ait-Si-Ali, and D. Trouche.** 2001. The histone deacetylase HDAC3 targets RbAp48 to the retinoblastoma protein. Nucleic Acids Res. **29**:3131–3136.
26. **Nicolas, E., V. Morales, L. Magnaghi-Jaulin, A. Harel-Bellan, H. Richard-Foy, and D. Trouche.** 2000. RbAp48 belongs to the histone deacetylase complex

that associates with the retinoblastoma protein. J. Biol. Chem. **275**:9797–9804.
27. **Oner, P., S. Bekpinar, F. Cinar, and A. Argun.** 1994. Relationship of some endogenous sex steroid hormones to leukocyte arylsulphatase A activities in pre- and postmenopausal healthy women. Horm. Metab. Res. **26**:301–304.
28. **Oren, M.** 2003. Decision making by p53: life, death and cancer. Cell Death Differ. **10**:431–442.
29. **Paramio, J. M., C. Segrelles, M. L. Casanova, and J. L. Jorcano.** 2000. Opposite functions for E2F1 and E2F4 in human epidermal keratinocyte differentiation. J. Biol. Chem. **275**:41219–41226.
30. **Pelzer, T., M. Schumann, M. Neumann, T. de Jager, M. Stimpel, E. Serfling, and L. Neyses.** 2000. 17β-Estradiol prevents programmed cell death in cardiac myocytes. Biochem. Biophys. Res. Commun. **268**:192–200.
31. **Petrovsky, N., D. Silva, L. Socha, R. Slattery, and B. Charlton.** 2002. The role of Fas ligand in beta cell destruction in autoimmune diabetes of NOD mice. Ann. N. Y. Acad. Sci. **958**:204–208.
32. **Pike, C. J.** 1999. Estrogen modulates neuronal Bcl-xL expression and beta-amyloid-induced apoptosis: relevance to Alzheimer's disease. J. Neurochem. **72**:1552–1563.
33. **Qian, Y. W., and E. Y. Lee.** 1995. Dual retinoblastoma-binding proteins with properties related to a negative regulator of ras in yeast. J. Biol. Chem. **270**:25507–25513.
34. **Qian, Y. W., Y. C. Wang, R. E. Jr. Hollingsworth, D. Jones, N. Ling, and E. Y. Lee.** 1993. A retinoblastoma-binding protein related to a negative regulator of Ras in yeast. Nature **364**:648-652.
35. **Rathmell, J. C., and C. B. Thompson.** 2002. Pathways of apoptosis in lymphocyte development, homeostasis, and disease. Cell **109**:S97–107.
36. **Rogoff, H. A., M. T. Pickering, M. E. Debatis, S. Jones, and T. F. Kowalik.** 2002. E2F1 induces phosphorylation of p53 that is coincident with p53 accumulation and apoptosis. Mol. Cell. Biol. **22**:5308–5318.
37. **Ruuls, S. R., R. M. Hoek, V. N. Ngo, T. McNeil, L. A. Lucian, M. J. Janatpour, H. Korner, H. Scheerens, E. M. Hessel, J. G. Cyster, L. M. McEvoy, and J. D. Sedgwick.** 2001. Membrane-bound TNF supports secondary lymphoid organ structure but is subservient to secreted TNF in driving autoimmune inflammation. Immunity **15**:533–543.
38. **Saegusa, K., N. Ishimaru, K. Yanagi, K. Mishima, R. Arakaki, T. Suda, I. Saito, and Y. Hayashi.** 2002. Prevention and induction of autoimmune exocrinopathy is dependent on pathogenic autoantigen cleavage in murine Sjogen's syndrome. J. Immunol. **169**:1050–1057.
39. **Saito, I., K. Haruta, M. Shimuta, H. Inoue, H. Sakurai, K. Yamada, N. Ishimaru, H. Higashiyama, T. Sumida, H. Ishida, T. Suda, T. Noda, Y. Hayashi, and K. Tsubota.** 1999. Fas ligand-mediated exocrinopathy resembling Sjogren's syndrome in mice transgenic for IL-10. J. Immunol. **162**: 2488–2494.
40. **Shirasuna, K., M. Sato, and T. Miyazaki.** 1981. A neoplastic epithelial duct cell line established form an irradiated human salivary gland. Cancer **48**: 745–752.
41. **Spyridopoulos, I., A. Sullivan, M. Kearney, J. Isner, and D. Losordo.** 1997. Estrogen-receptor-mediated inhibition of human endothelial cell apoptosis. Estradiol as a survival factor. Circulation **95**:1505–1514.
42. **Stassi, G., and R. De Maria.** 2002. Autoimmune thyroid disease: new models of cell death in autoimmunity. Nat. Rev. Immunol. **2**:195–204.
43. **Szende, B., I. Romics, and L. Vass.** 1993. Apoptosis in prostate cancer after hormonal treatment. Lancet **342**:1422.
44. **Tan, X., and J. Y. J. Wang.** 1998. The caspase-RB connection in cell death. Trends Cell Biol. **8**:116–120.
45. **Vanags, D. M., M. I. Porn-Ares, S. Coppola, D. H. Burgess, and S. Orrenius.** 1996. Protease involvement in fodrin cleavage and phosphatidylserine exposure in apoptosis. J. Biol. Chem. **271**:31075–31085.
46. **Vaute, O., E. Nicolas, L. Vandel, and D. Trouche.** 2002. Functional and physical interaction between the histone methyl transferase Suv39H1 and histone deacetylases. Nucleic Acids Res. **30**:475–481.
47. **Vousden, K. H.** 2000. p53: death star. Cell **103**:691–694.
48. **Wang, K. K., R. Posmantur, R. Nath, K. McGinnis, M. Whitton, R. V. Talanian, S. B. Glantz, and J. S. Morrow.** 1998. Simultaneous degradation of αII- and βII-spectrin by caspase 3 (CPP32) in apoptotic cells. J. Biol. Chem. **273**:22490–22497.
49. **Wang, R. H., C. W. Liu, V. L. Avramis, and N. Berndt.** 2001. Protein phosphatase 1α-mediated stimulation of apoptosis is associated with dephosphorylation of the retinoblastoma protein. Oncogene **20**:6111–6122.
50. **Whitacre, C. C.** 2001. Sex differences in autoimmune disease. Nat. Immunol. **2**:777–780.
51. **Whitacre, C. C., S. C. Reingold, and P. A. O'Looney.** 1999. A gender gap in autoimmunity. Science **283**:1277–1278.
52. **Yu, J. Y., S. L. DeRuiter, and D. L. Turner.** 2002. RNA interference by expression of short-interfering RNAs and hairpin RNAs in mammalian cells. Proc. Natl. Acad. Sci. USA **99**:6047–6052.
53. **Zhang, Q., N. Vo, and R. H. Goodman.** 2000. Histone binding protein RbAp48 interacts with a complex of CREB binding protein and phosphorylated CREB. Mol. Cell. Biol. **20**:4970–4978.
54. **Zhang, Y., B. O'Brien, J. Trudeau, R. Tan, P. Santamaria, and J. P. Dutz.** 2002. In situ β cell death promotes priming of diabetogenic CD8 T lymphocytes. J. Immunol. **168**:1466–1472.

Immunity 24, 165–177, February 2006 ©2006 Elsevier Inc. DOI 10.1016/j.immuni.2005.12.011

CCR7-Dependent Cortex-to-Medulla Migration of Positively Selected Thymocytes Is Essential for Establishing Central Tolerance

Hirotsugu Kurobe,[1,2] Cunlan Liu,[1] Tomoo Ueno,[1,5] Fumi Saito,[1] Izumi Ohigashi,[1] Natalie Seach,[5] Rieko Arakaki,[3] Yoshio Hayashi,[3] Tetsuya Kitagawa,[2] Martin Lipp,[4] Richard L. Boyd,[5] and Yousuke Takahama[1,*]

[1]Division of Experimental Immunology
Institute for Genome Research
University of Tokushima
Tokushima 770-8503
Japan

[2]Department of Cardiovascular Surgery

[3]Department of Oral Molecular Pathology
Institute of Health Biosciences
University of Tokushima
Tokushima 770-8503
Japan

[4]Department of Molecular Tumorgenetics and Immunogenetics
Max-Delbrück Center for Molecular Medicine
Berlin 13125
Germany

[5]Monash Immunology and Stem Cell Laboratories
Monash University
Clayton 3800
Victoria
Australia

Summary

Immature CD4$^+$CD8$^+$ thymocytes, which are generated in the thymic cortex, are induced upon positive selection to differentiate into mature T lymphocytes and relocate to the thymic medulla. It was recently shown that a chemokine signal via CCR7 is essential for the cortex-to-medulla migration of positively selected thymocytes in the thymus. However, the role of the cortex-to-medulla migration in T cell development and selection has remained unclear. The present study shows that the developmental kinetics and the thymic export of mature thymocytes were undisturbed in adult mice lacking CCR7 or its ligands (CCR7L). The inhibition of sphingosine-1-phosphate-mediated lymphocyte egress from the thymus led to the accumulation of mature thymocytes in the cortex of CCR7- or CCR7L-deficient mice, unlike the accumulation in the medulla of normal mice, thereby suggesting that mature thymocytes may be exported directly from the cortex in the absence of CCR7 signals. However, the thymocytes that were generated in the absence of CCR7 or CCR7L were potent in causing autoimmune dacryoadenitis and sialadenitis in mice and were thus incapable of establishing central tolerance to organ-specific antigens. These results indicate that CCR7-mediated cortex-to-medulla migration of thymocytes is essential for establishing central tolerance rather than for supporting the maturation or export of thymocytes.

*Correspondence: takahama@genome.tokushima-u.ac.jp

Introduction

The thymus is an organ that supports the differentiation and selection of T lymphocytes (Miller, 1961; Ritter and Boyd, 1993; Anderson and Jenkinson, 2001). Lymphoid progenitor cells enter the thymus via the surrounding mesenchymal layer before vascularization during fetal development (Bleul and Boehm, 2000) and via blood vessels that are enriched at the cortico-medulla junction in adulthood (Lind et al., 2001). Several chemokines have been suggested to play a crucial role in the positioning of T precursor cells to the subcapsular zone of the outer cortex of the thymus (Plotkin et al., 2003; Misslitz et al., 2004; Benz et al., 2004; Gray et al., 2005; Liu et al., 2005), where immature CD4$^+$CD8$^+$ double-positive (DP) thymocytes are newly generated (Ritter and Boyd, 1993; Takahama et al., 1994). The DP thymocytes crawl through the cortical environment, seeking to encounter the self-MHC-peptide complex expressed by various stromal cells in the cortex, including the cortical thymic epithelial cells (cTEC) (Bousso et al., 2002). Upon TCR engagement by the MHC-peptide ligands, the DP thymocytes stop crawling and initiate the signaling processes for positive and negative selection, which result in further differentiation into CD4$^+$CD8$^-$/CD4$^-$CD8$^+$ single-positive (SP) thymocytes and apoptotic deletion, respectively (Bousso et al., 2002; Palmer, 2003). Concurrently to the differentiation into SP thymocytes, positively selected thymocytes are relocated to the medulla (Ritter and Boyd, 1993; van Ewijk et al., 1994; Witt et al., 2005). The newly generated SP thymocytes are semimature, being functionally incompetent and susceptible to various apoptotic signals including dexamethasone, and undergo further maturation to become mature SP thymocytes that are functional, dexamethasone-resistant, and CD62L^{high}CD69^{low} (Reichert et al., 1986a; Ramsdell et al., 1991; Kishimoto and Sprent, 1997; Gabor et al., 1997; Sheard et al., 2004). The mature SP thymocytes are exported from the thymus via chemotaxis toward sphingosine-1-phosphate (S1P) in the circulation and are systemically distributed as functional yet naive T lymphocytes (Matloubian et al., 2004; Allende et al., 2004). The maturation of SP thymocytes is thought to occur within the medulla (Egerton et al., 1990; Scollay and Godfrey, 1995), and the export to the circulation is thought to occur through the perivascular space in the medulla (Ushiki, 1986; Kato, 1997).

In the thymic medulla, medullary thymic epithelial cells (mTEC) specifically express the nuclear protein AIRE, which is essential for the promiscuous expression of organ-specific self-antigens by mTEC (Zuklys et al., 2000; Gotter and Kyewski, 2004). AIRE deficiency results in autoimmune-polyendocrinopathy-candidiasis ectodermal dystrophy (APECED) in human (Nagamine et al., 1997; Aaltonen et al., 1997) and mouse (Anderson et al., 2002; Liston et al., 2003; Kuroda et al., 2005). Thus, AIRE expressed by mTEC is essential for establishing the central tolerance of T lymphocytes to organ-specific antigens. The molecular mechanisms involved in the differentiation of thymic epithelial progenitor cells into

AIRE-expressing mTEC have remained vague (Blackburn et al., 2002; Farr et al., 2002), although recent analyses have shown that similar to the organogenesis of lymph nodes and Peyer's patches, the NFκB-mediated signals via LTβR, TRAF6, NIK, and relB are critical for the development of the thymic medulla that regulates central tolerance (Burkly et al., 1995; Boehm et al., 2003; Kajiura et al., 2004; Akiyama et al., 2005). It has also been suggested that the thymic medulla contributes to central tolerance by dendritic cells (DCs), which are of hematopoietic origin and are predominantly localized within the thymic medulla (Flotte et al., 1983; Fairchild and Austyn, 1990). The average lifespan of the newly generated SP thymocytes in the thymus is 12 days (Egerton et al., 1990; Scollay and Godfrey, 1995). During this period, the thymic medulla is thought to provide an environment in which the SP thymocytes are induced to mature and are tuned to acquire central tolerance. However, whether the medulla migration of positively selected thymocytes is essential for the maturation of SP thymocytes, for the acquisition of central tolerance, or for the export from the thymus is unclear.

Previous studies with the chemotaxis assay and mRNA measurement showed that CCR7 expression by developing thymocytes is associated with the phenotypic stage of cortex-to-medulla migration, during the development of immature DP thymocytes to mature SP thymocytes (Kim et al., 1998; Campbell et al., 1999). We have recently shown that CCR7 ligands (CCR7L species CCL19 and CCL21) in the thymus are predominantly produced by mTEC and are localized in the medulla, whereas TCR engagement of immature cortical DP thymocytes elevates the cell surface expression of CCR7 (Ueno et al., 2002, 2004). In mice deficient in CCR7 or CCR7L, the mature SP thymocytes are arrested in the cortex and do not accumulate in the medulla (Ueno et al., 2004). These results indicate that the CCR7 signals are essential for the migration of positively selected thymocytes from the cortex to the medulla. By using mice that are deficient in CCR7 or CCR7L, the present study addresses whether T cells may be exported from the thymic cortex without accumulation in the medulla and whether central tolerance to organ-specific self-antigens may be affected by the absence of medulla migration. We show that the pharmacological inhibition of S1P-mediated thymocyte egress in CCR7- or CCR7L-deficient mice results in the accumulation of mature thymocytes in the cortex, suggesting that mature thymocytes may be exported via the S1P-dependent mechanism from the cortex in the absence of CCR7 signals. We also show that in the absence of CCR7-dependent medulla migration, mature thymocytes are incapable of acquiring tolerance to lacrimal and salivary glands and are potent in inducing autoimmune exocrinopathy similar to Sjögren's syndrome.

Results

S1P Blockade Induces Accumulation of Mature Thymocytes in the Thymic Cortex of CCR7- or CCR7L-Deficient Mice

We have previously shown that mice deficient in CCR7 or CCR7L were defective in the cortex-to-medulla migration of thymocytes and that SP thymocytes generated in CCR7L-deficient (*plt/plt*, P/P) or CCR7-deficient (7/7) mice were barely accumulated in the thymic medulla (Ueno et al., 2004). SP thymocytes in these mutant mice appeared normal in terms of frequency and underwent maturation, including TCR responsiveness and formation of surface phenotypes such as CD62L and CD69 (Ueno et al., 2004). In vivo 5-bromo-2-deoxyuridine (BrdU) labeling showed that SP thymocytes and DP thymocytes in these mutant mice were normally generated according to the developmental kinetics (Figure 1A). In addition, intrathymic FITC administration showed that SP thymocytes in CCR7L- or CCR7-deficient mice were normally exported from the adult thymus to the circulation (Ueno et al., 2004). These results indicate that in CCR7L- or CCR7-deficient adult mice, SP thymocytes show normal maturation without medulla accumulation and normal export from the thymus.

The above results suggested the possibility that the mature SP thymocytes generated in CCR7- or CCR7L-deficient mice might be exported from the cortex without migrating into the medulla. In order to examine this possibility, the mice were administered FTY720, an immunosuppressive compound that is phosphorylated in vivo by sphingosine kinases and acts as an S1P mimetic to sequester T lymphocytes in the thymus and lymph nodes (Chiba et al., 1998; Brinkmann et al., 2002). It was previously shown that S1P1, one of the S1P receptors, is expressed by mature SP thymocytes and that S1P1 is required for the egress of T lymphocytes from the thymus and lymph nodes (Matloubian et al., 2004; Allende et al., 2004). Among the thymocyte subpopulations, S1P1 mRNA was highly expressed in SP thymocytes rather than DP or double-negative (DN) thymocytes (Matloubian et al., 2004; Allende et al., 2004; also shown in Figure 1B). Within the SP thymocytes, the S1P1 expression was predominantly detected in the $CD62L^{high}CD69^{low}$ mature subpopulation rather than the $CD62L^{low}CD69^{high}$ semimature subpopulation (Matloubian et al., 2004; also shown in Figure 1B). Similar to S1P1 expression, CCR7 expression was much higher in SP thymocytes than in DP or DN thymocytes (Kwan and Killeen, 2004; Misslitz et al., 2004; also shown in Figure 1B). Unlike S1P1 expression, however, CCR7 expression was detected in $CD62L^{low}CD69^{high}$ semimature thymocytes as well as in $CD62L^{high}CD69^{low}$ mature thymocytes (Figure 1B). The CCR7 mRNA expression levels measured by quantitative RT-PCR analysis agreed with the CCR7 surface expression levels measured by flow cytometry analysis with CCL19-Ig fusion protein (Figures 1C and 1D). $CCR7^{high}TCR\beta^{high}$ thymocytes contained both the $CD62L^{low}CD69^{high}$ semimature compartment and the $CD62L^{high}CD69^{low}$ mature compartment, whereas $CCR7^{negative/low}TCR\beta^{high}$ thymocytes predominantly contained the $CD62L^{low}CD69^{high}$ semimature compartment (Figure 1C). CCR7 expression was higher in $CD62L^{high}CD69^{low}$ mature thymocytes than in $CD62L^{low}CD69^{high}$ semimature thymocytes (Figure 1D). These results indicate that CCR7 expression is detected in both $CD62L^{low}CD69^{high}$ semimature and $CD62L^{high}CD69^{low}$ mature thymocytes, whereas S1P1 expression is detected predominantly in the $CD62L^{high}CD69^{low}$ mature subpopulation,

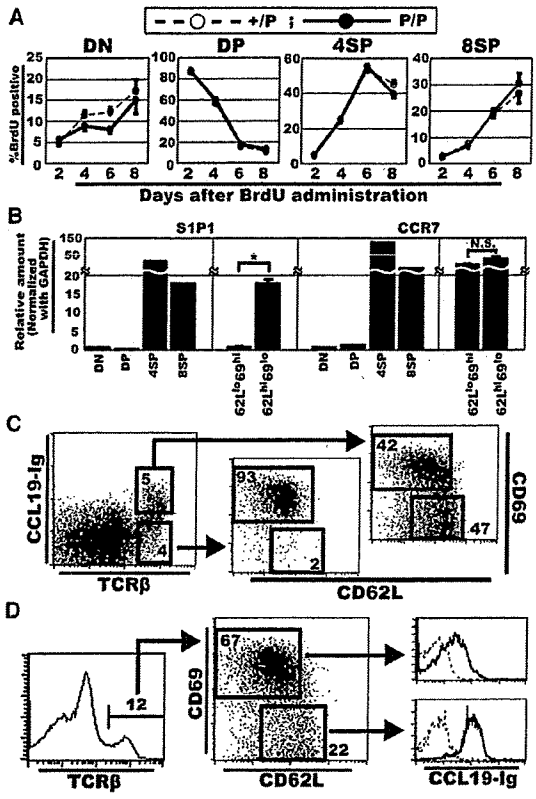

Figure 1. Expression and Function of CCR7 in Thymocyte Subpopulations

(A) Kinetics of mature thymocytes in mice deficient in CCR7L (*plt/plt*, P/P) and their heterozygous control mice (+/P). Thymocytes from BrdU-treated adult mice were stained for CD4, CD8, and BrdU. Plots show means and standard deviations (symbols and bars, respectively; the number of mice used for individual plots ranged from five to seven) of the frequency of BrdU-positive cells within the indicated CD4/CD8 populations of thymocytes on the indicated day of analysis. All the data sets between +/P and P/P groups were not significantly different at all the indicated days of analysis in all of the indicated thymocyte subpopulations (including the data on DN thymocytes) by the Student's t test.

(B) Adult thymocytes from B6 mice were two-color stained for CD4 and CD8 and sorted for DN, DP, CD4SP, and CD8SP populations. Adult B6 thymocytes were also three-color stained for TCRβ, CD62L, and CD69 and were sorted for $TCR\beta^{high}CD62L^{low}CD69^{high}$ semimature and $TCR\beta^{high}CD62L^{high}CD69^{low}$ mature subpopulations. Purity was >97% for CD4/CD8 two-color-sorted fractions and >87% for TCRβ/CD62L/CD69 three-color-sorted fractions. Relative mRNA levels (means and standard errors; n = 3) obtained by quantitative RT-PCR for S1P1 and CCR7, which were normalized to GAPDH mRNA levels, are shown. Asterisk indicates $p < 0.05$ by the Student's t test. N.S., not significant.

(C and D) Adult B6 thymocytes were examined for CCR7 surface expression by using CCL19-Ig, which specifically detects CCR7 on the cell surface. Cells were also stained with PE-labeled anti-TCRβ antibody, FITC-labeled anti-CD62L antibody, and PE-Cy5-labeled anti-CD69 antibody. Where indicated, data were gated for $TCR\beta^{high}CCR7^{high}$ and $TCR\beta^{high}CCR7^{negative/low}$ cells (C) and $TCR\beta^{high}CD62L^{low}CD69^{high}$ and $TCR\beta^{high}CD62L^{high}CD69^{low}$ cells (D). Numbers indicate frequencies of cells within the indicated boxes. Dotted lines indicate control staining profiles without CCL19-Ig. Shown are representative results of four independent measurements.

suggesting that the CCR7-mediated medulla migration and the S1P1-mediated thymocyte egress are differently and sequentially regulated during SP thymocyte maturation.

Importantly, FTY720 treatment induced the accumulation of SP thymocytes in CCR7- or CCR7L-deficient mice as well as in normal mice (Figures 2A and 2B). Among the SP thymocytes, the accumulation was specifically induced in the $CD62L^{high}CD69^{low}$ mature population, in either the CD4SP or the CD8SP compartment (Figures 2A and 2C). Thus, the FTY720-mediated S1P blockade of thymocyte egress to the circulation results in the accumulation of $CD62L^{high}$ mature SP thymocytes even in CCR7- or CCR7L-deficient mice, in which most SP thymocytes are arrested in the cortex and are defective in migrating into the medulla.

It was therefore interesting to identify the location in the thymus where mature thymocytes were accumulating upon FTY720 treatment in CCR7- or CCR7L-deficient mice, as the location for this accumulation would correspond to the microenvironment where S1P would otherwise act to attract mature thymocytes into the circulation. To this end, thymus sections from FTY720-treated mice were stained with mature-thymocyte-specific anti-CD62L antibody and either mTEC-specific ER-TR5 or cTEC-specific ER-TR4 monoclonal antibodies (Figure 3). In agreement with the increase in the $CD62L^{high}$ SP thymocyte population as determined by flow cytometry analysis (Figure 2C), the FTY720 treatment markedly increased the $CD62L^{high}$ thymocyte population in normal mice as well as in CCR7- or CCR7L-deficient mice (Figure 3A). In a parallel analysis of the sections, the increased $CD62L^{high}$ cells were indeed shown to belong to CD4 or CD8 single-positive thymocytes in normal and mutant mice (data not shown), indicating that the $CD62L^{high}$ thymocytes increased in Figure 3A represented mature SP thymocytes. Most remarkably, the FTY720-mediated accumulation of $CD62L^{high}$ mature thymocytes was predominantly detected in the cortex and not the medulla of CCR7- or CCR7L-deficient mice, whereas the $CD62L^{high}$ mature thymocytes were accumulated predominantly in the medulla of control mice (Figure 3A). In the cortex of FTY720-mediated CCR7- or CCR7L-deficient mice and in the medulla of FTY720-mediated control mice, the analysis at higher magnification detected areas where $CD62L^{high}$ thymocytes accumulated around $CD31^+$ endothelial vessels (Figure 3B). In some of those areas, $CD62L^{high}$ thymocytes were found even within the perivascular space surrounded by $CD31^+$ endothelial and $ER\text{-}TR7^+$ mesenchymal cells (Figure 3C). In contrast, no or very few $CD62L^{high}$ thymocytes were found in the medulla of FTY720-treated CCR7- or CCR7L-deficient mice and in the cortex of FTY720-treated control mice (Figures 3A, 3B, and 3C). These results indicate that upon FTY720 treatment, the mature SP thymocytes in CCR7- or CCR7L-deficient mice are accumulated in the cortex rather than the medulla of the thymus and are found even in the cortical perivascular space, suggesting the possibility that mature thymocytes generated in CCR7- or CCR7L-deficient mice may be exported from the cortex through the cortical perivascular space in a S1P-dependent manner.

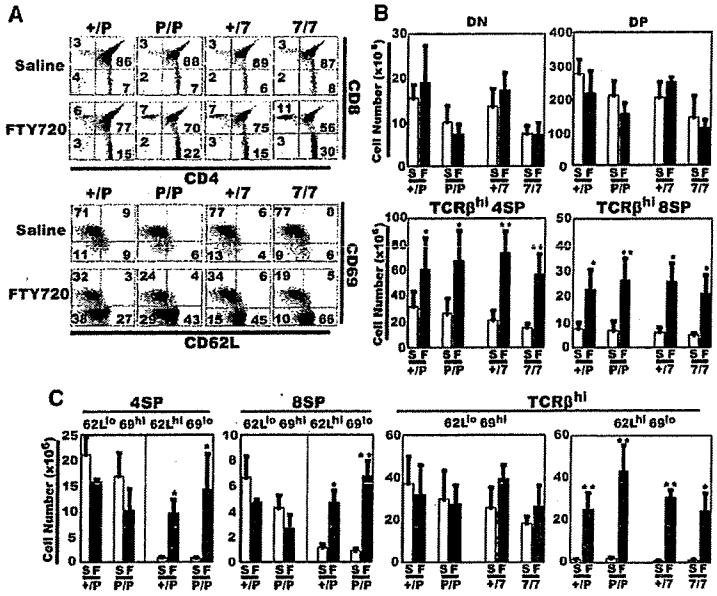

Figure 2. Accumulation of Mature Thymocytes by FTY720-Mediated S1P Blockade

Flow cytometry analysis of thymocytes from CCR7L-deficient mice (*plt/plt*, P/P), CCR7-deficient mice (7/7), and their heterozygous control mice (+/P and +/7), which were treated with either saline (S) or FTY720 (F). The profiles of CD62L and CD69 in (A) were gated for $TCR\beta^{hi/gh}$ cells. Numbers in (A) indicate frequencies of cells within the quadrants.

(B and C) Means and standard errors (the numbers of mice analyzed ranged from four to 11 in [B] and three to six in [C]) of the absolute numbers of indicated thymocyte subpopulations are shown. Asterisk indicates $p < 0.05$ and double asterisk indicates $p < 0.005$ by the Student's t test.

Intrathymic Localization of AIRE$^+$ Epithelial Cells and Dendritic Cells in CCR7- or CCR7L-Deficient Mice

We then addressed whether thymic function in inducing central tolerance is affected in CCR7- or CCR7L-deficient mice. It was previously reported that the thymic medulla contributes to establishing central tolerance by AIRE-expressing mTEC (Zuklys et al., 2000; Anderson et al., 2002; Liston et al., 2003; Kuroda et al., 2005) and medulla-localized DCs (Fairchild and Austyn, 1990; Moore et al., 1994). We thus examined whether AIRE$^+$ mTEC and CD11c$^+$ DCs were indeed localized within the medulla in CCR7- or CCR7L-deficient mice. Figure 4 shows that AIRE$^+$ cells in the thymus were predominantly confined in the medullary region in CCR7- or CCR7L-deficient mice as well as in normal mice (Figures 4A and 4B). The analysis at high magnification showed that in the thymus of CCR7- or CCR7L-deficient mice as well as in normal mice, AIRE expression was found in the nuclei, as previously reported (Bjorses et al., 1999; Rinderle et al., 1999), and in a fraction of keratin$^+$MTS-10$^+$ mTEC (Figure 4C). It was also shown that in CCR7- or CCR7L-deficient mice, as in normal mice, CD11c$^+$ DCs were predominantly localized in the medulla, although some CD11c$^+$ DCs were sparsely found in the cortex even in normal mice (Figures 4D and 4E). These results indicate that similar to that of normal mice, AIRE in the thymus of CCR7- or CCR7L-deficient mice are predominantly expressed in the medulla by a fraction of mTEC. The results also show that DCs in the thymus are enriched in the medulla in CCR7- or CCR7L-deficient mice, indicating that CCR7 signals are not required for the accumulation of DCs in the thymic medulla. The results suggest that developing thymocytes in CCR7- or CCR7L-deficient mice, which are not accumulated in the medulla, may fail to directly interact with AIRE$^+$ mTEC.

Thymocytes Generated in CCR7L-Deficient Mice Are Potent in Inducing Autoimmune Exocrinopathy

The above results raised the possibility that the establishment of thymic-medulla-dependent central tolerance to organ-specific antigens might be affected in CCR7- or CCR7L-deficient mice. We thus examined various organs of these mutant mice for lesions that might be associated with defective self-tolerance. As shown in Figure 5, we found that the lacrimal glands, the parotid glands, and the submandibular glands exhibited periductal lymphocyte infiltration in CCR7- or CCR7L-deficient mice (Figures 5A, 5B, and 5C). Lymphocyte infiltration in the lacrimal glands was accompanied by severe tissue damage, including the destruction of acinar cells (Figures 5A and 5D and Figure 6A). In mice up to 25 weeks old, the tissue damage was largely specific for these exocrine glands, as no apparent lesions were detected in other organs, including the trachea, thyroid, liver, spleen, kidney, intestine, adrenal gland, and ovary (data not shown). The lesions in these exocrine glands were detected in all the tested mutant mice ($n = 14$ for *plt/plt* mice; $n = 5$ for CCR7-deficient mice), even as early as 5 weeks old (Figure 5D), and were found similarly in CCR7L-deficient mice of BALB/c background as well as C57BL/6 background (Figures 5A, 5B, and 5C). The infiltrated lymphocytes were mostly CD4$^+$ T cells and B cells, and tissue-reactive antibodies were markedly deposited in the damaged tissues (Figures 6B and 6C). These results indicate that CCR7- or CCR7L-deficient mice exhibit autoimmune exocrinopathy resembling Sjögren's syndrome.

To examine whether the autoimmune exocrinopathy is a direct consequence of the defect in thymocytes, the CCR7L-deficient *plt/plt* thymocytes were transferred into RAG2-deficient mice that lacked T cells and B cells. Under this experimental condition, the *plt/plt*

thymocytes were not defective in CCR7 expression, and the host RAG2-deficient mice were not defective in CCR7L expression. CCR7-expressing *plt/plt*-derived T cells would normally migrate to CCR7L-expressing host tissues, including lymph nodes and exocrine glands, in the RAG2-deficient mice. Thus, the defect in CCR7/CCR7L signaling in this cell transfer experiment would be limited to the period of thymocyte development before the cell transfer, and the transferred thymocyte-derived T cells would exhibit no or little aberrancy in the peripheral distribution after the cell transfer. As shown in Figures 7A and 7B, the transfer of CCR7L-deficient *plt/plt* thymocytes as well as *plt/plt* spleen cells caused significant lymphocyte infiltration in the lacrimal and salivary glands. By contrast, the transfer of control *+/plt* thymocytes or *+/plt* spleen cells did not cause such lymphocyte infiltration (Figures 7A and 7B). These results indicate that the thymocytes generated without CCR7L are potent in inducing autoimmune exocrinopathy in mice and, thus, are defective in establishing central tolerance.

It was previously shown that *plt/plt* or CCR7-deficient mice are defective in forming the medullary architecture characterized by clusters of UEA-1$^+$ cells (Ueno et al., 2004). We finally addressed whether the defective central tolerance in the thymus lacking CCR7 or CCR7L is due to defective thymocyte accumulation in the medulla or defective architecture of the medullary stroma. To this end, we generated mixed bone marrow chimeras reconstituted with equal numbers of bone marrow cells from CCR7-deficient mice and normal mice and examined whether these mixed bone marrow chimeras might exhibit the autoimmune exocrinopathy. Due to the presence of normal bone-marrow-derived thymocytes, it was presumed that the medullary architecture in the mixed bone marrow chimeras would appear normal even in the presence of CCR7-deficient thymocytes. Indeed, normal architecture of the medullary region containing the UEA-1$^+$ clusters was detected in the mixed bone marrow chimeras, which was similar to that in the normal bone marrow chimeras and different from that in CCR7-deficient bone marrow chimeras (Figure 7C), whereas the accumulation of CD45.2$^+$ CCR7-deficient thymocytes in the medulla was severely defective in the mixed bone marrow chimeras (Figure 7D). However, these mixed bone marrow chimeras exhibited the autoimmune phenotypes in the lacrimal glands, including lymphocyte infiltration and tissue damage, similar to the bone marrow chimeras reconstituted with CCR7-deficient bone marrow cells alone (Figures 7E and 7F). These results indicate that CCR7-deficient bone-marrow-derived cells that are reconstituted in the normal thymus architecture are potent in inducing autoimmune exocrinopathy, suggesting that the autoimmune phenotype in CCR7-deficient mice is likely due to the lack of thymocyte accumulation in the medulla rather than the defective development of the medullary architecture. These results also indicate that CCR7-deficient bone-marrow-derived cells that are reconstituted in the presence of normally developing hematopoietic cells are still potent in inducing autoimmune exocrinopathy, suggesting that the autoimmunity in these mutant mice may be caused even in the presence of normally generated immune cells, including regulatory T cells.

Discussion

The present results show that mature thymocytes are normally generated in developmental kinetics and are normally exported in CCR7- or CCR7L-deficient adult mice. The pharmacological inhibition of S1P-mediated thymocyte egress shows that in the absence of CCR7 signals, the mature thymocytes are accumulated in the thymic cortex rather than the thymic medulla, suggesting that the S1P-mediated thymocyte egress may occur in the thymic cortex of these mutant mice. These results argue the possibility that the thymic medulla may not be required for the maturation or export of thymocytes. On the other hand, our results also show that in the absence of CCR7 signals, the mature thymocytes are incapable of acquiring tolerance to lacrimal and salivary glands and are potent in inducing autoimmune exocrinopathy. Thus, CCR7-mediated cortex-to-medulla migration of positively selected thymocytes is essential for establishing central tolerance rather than for supporting the maturation or export of thymocytes.

The Cortex and Thymocyte Export

Our results show that the developmental kinetics and the thymic export of SP thymocytes are undisturbed in adult mice lacking CCR7 or CCR7L. FTY720 treatment shows that the mature thymocytes are accumulated in the thymic cortex of CCR7- or CCR7L-deficient mice, unlike the accumulation in the medulla of normal mice. FTY720-sensitive S1P-dependent chemotaxis is essential for the egress of mature thymocytes to the circulation (Matloubian et al., 2004). Thus, the present results suggest that the mature thymocytes generated in CCR7- or CCR7L-deficient mice may be exported from the cortex without migrating into the medulla. It has been generally thought that the medulla is a place for the maturation and export of thymocytes (Ritter and Boyd, 1993; Scollay and Godfrey, 1995; Anderson and Jenkinson, 2001). Indeed, our results from the FTY720 treatment of normal mice agree with the notion that S1P-dependent thymocyte export occurs in the medulla of normal mice (Figure 3). However, our results also suggest the possibility that in the case that the positively selected thymocytes remain in the cortex without being attracted to CCR7L expressed in the medulla, the thymic cortex can not only nurture the maturation of SP thymocytes but also export the mature thymocytes. Based on these results, we propose the possibility that the thymic cortex may have the capability of fully supporting the development of T cells, including SP thymocyte maturation and the export of mature T cells. This possibility is consistent with previous findings that T cell maturation and peripheral supply are not perturbed in relB-deficient mice that lack the thymic medulla (Burkly et al., 1995).

It should be noted that we detected a minor fraction of mature SP thymocytes in the medullary areas of CCR7- or CCR7L-deficient mice (Ueno et al., 2004). However, FTY720 treatment does not cause the accumulation of mature thymocytes in the medulla of CCR7- or CCR7L-deficient mice (Figure 3), arguing the possibility that those medullary thymocytes in CCR7- or CCR7L-deficient mice do not represent mature thymocytes whose S1P-dependent egress from the thymus is blocked. It is even unclear whether those medullary thymocytes in

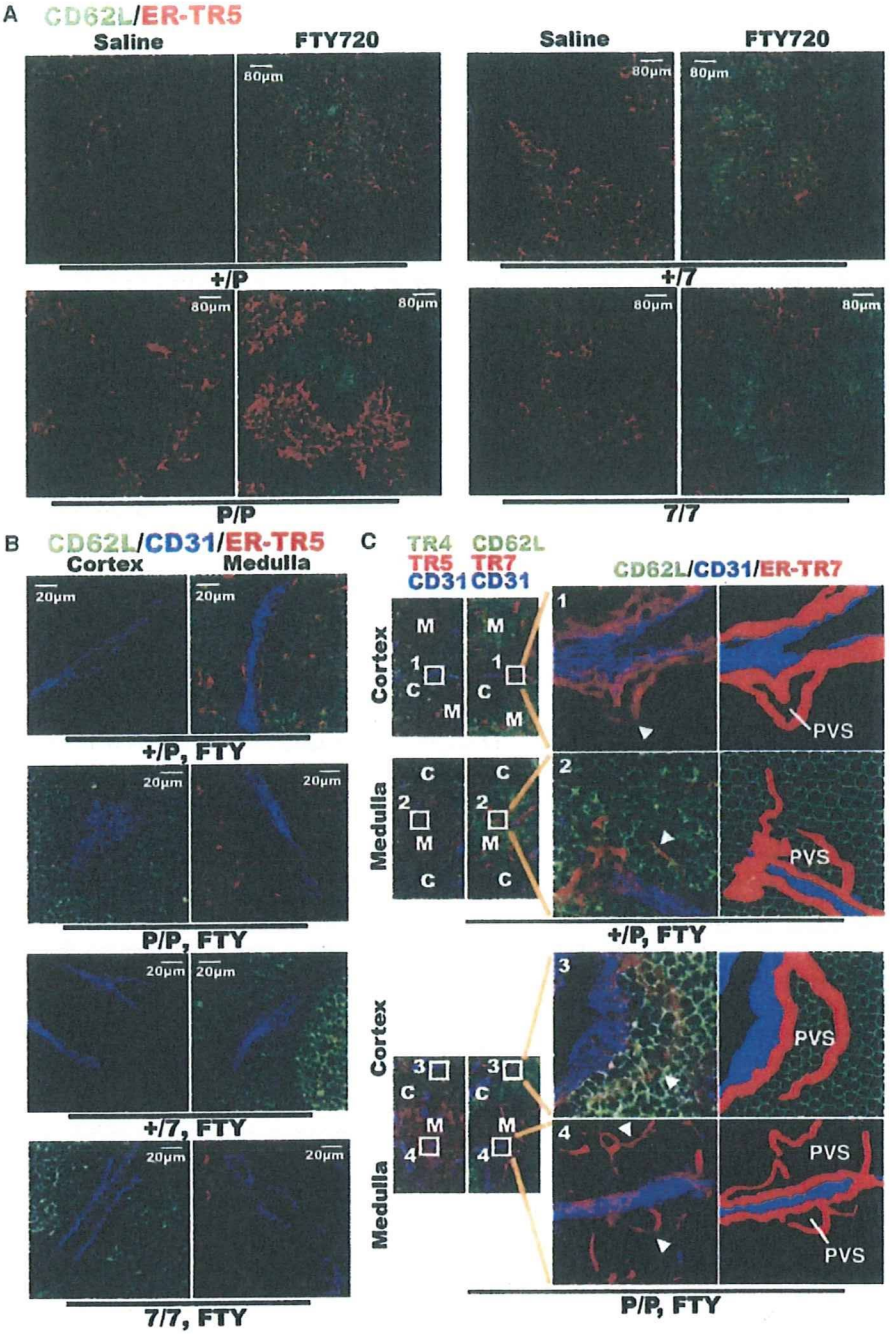

Figure 3. FTY720-Mediated Accumulation of Mature Thymocytes in the Thymic Cortex of CCR7- or CCR7L-Deficient Mice

Frozen sections of the thymus from indicated mice were two-color or three-color stained for CD62L (green) and mTEC-specific ER-TR5 (red) (A); CD62L (green), CD31 (blue), and ER-TR5 (red) (B); ER-TR4 (green), CD31 (blue), and ER-TR5 (red) (C); or CD62L (green), CD31 (blue), and ER-TR7 (red) (C), as indicated. The cortex and the medulla in (B) were identified by staining of the adjacent sections with cTEC-specific ER-TR4 and mTEC-specific ER-TR5. The high magnification images in (B) show that in the cortex of FTY720-mediated CCR7L-deficient mice (P/P) and CCR7-deficient mice (7/7) and in the medulla of FTY720-mediated control mice (+/P and +/7), there are the areas where many CD62L^{high} thymocytes were accumulated around CD31^{+} endothelial vessels. It should be noted that low-magnification images of the cortex in the FTY720-treated mutant mice (P/P and 7/7) and of the medulla in the FTY720-treated control mice (+/P and +/7) show that not all areas in the cortex are uniformly filled with CD62L^{high} thymocytes and that there are also the cortical areas where only a few CD62L^{high} thymocytes were found (A). On the other hand, no or very few CD62L^{high} thymocytes were found in the medulla of FTY720-mediated CCR7- or CCR7L-deficient mice (P/P and 7/7) and in the cortex of FTY720-mediated control mice (+/P and +/7) in low-magnification as well as in high-magnification images (A and B).

(C) Serial sections were stained as indicated. The cortex (C) and the medulla (M) were identified by ER-TR4 and ER-TR5. The perivascular space (PVS) was identified as the areas surrounded by CD31^{+} endothelial and ER-TR7^{+} mesenchymal cells. High-magnification images of boxes 1, 2, 3,

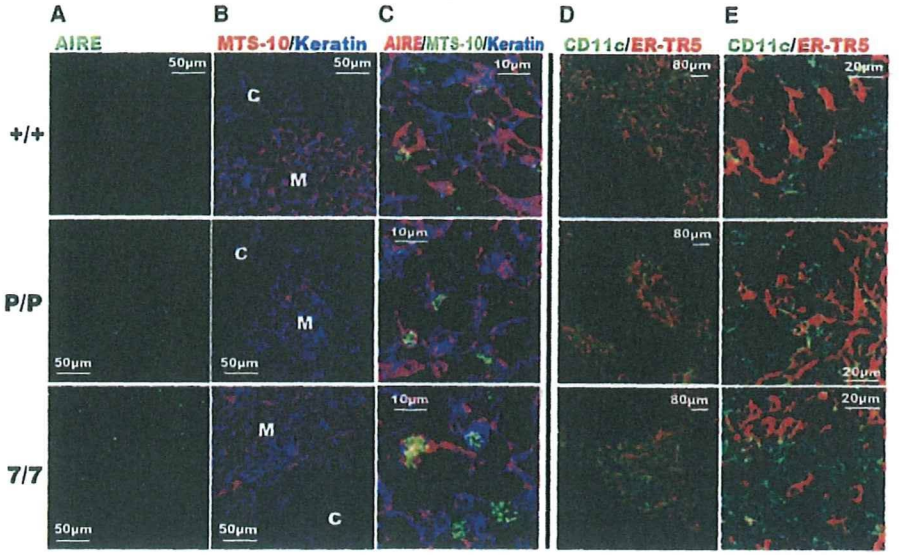

Figure 4. Intrathymic Distribution of AIRE-Expressing Cells and DCs in CCR7- or CCR7L-Deficient Mice

(A–C) Thymus sections from B6 (+/+), *plt/plt* (P/P), and CCR7-deficient (7/7) adult mice were stained with anti-AIRE (green), anti-keratin (blue), and mTEC-specific MTS-10 (red) antibodies. Cortex (C) and medulla (M) were identified with MTS-10 staining (B). High-magnification images from the three-color staining in (C) show that AIRE, keratin, and the MTS-10 determinant in the mutant mice as well as in the control mice are expressed in single mTEC, although AIRE is selectively localized in the nuclei whereas keratin and MTS-10 determinants are predominantly localized at the cytoplasm and the plasma membrane, respectively.

(D and E) Thymus sections from indicated mice were also stained for CD11c (green) and ER-TR5 (red).

Shown are representative results of more than three independent analyses.

the mutant mice may represent mature thymocytes that will eventually be exported from the thymus. Nevertheless, it is possible that some mature thymocytes in CCR7- or CCR7L-deficient mice may egress from the thymus through the medullary and/or cortico-medullary junction areas.

Perhaps, however, it is more tempting to speculate that the minor fraction of mature thymocytes found in the medulla of CCR7- or CCR7L-deficient mice may contribute to the crosstalk signals to induce the generation of AIRE$^+$ mTEC in the medullary area. It was previously shown that the generation of mature SP thymocytes is essential for the development of the medullary epithelial architecture (van Ewijk et al., 1994). On the other hand, CCR7- or CCR7L-deficient mice generate the thymus with a small but distinct medullary region (Ueno et al., 2004) that contains AIRE$^+$ mTEC as well as DCs (Figure 4), even though the generation of UEA-1$^+$ clusters in the medulla is impaired (Ueno et al., 2004; also shown in Figure 7 of this study). Thus, it is possible that the CCR7-independent migration into the medulla by a small fraction of mature thymocytes may play a role in the development of TEC precursor cells to generate AIRE$^+$ mTEC and the localization of DCs in the medulla.

The perivascular space in the postnatal thymus is distributed around the venules and some arterioles and is enriched in the medulla and the cortico-medullary junction (Ushiki, 1986; Kato, 1997). However, the perivascular space is also found within the cortex in normal animals (Ushiki, 1986; Kato, 1997; F.S. and Y.T., unpublished data). It has been speculated that the perivascular space is a route for T cell egress from the thymus parenchyma to the circulation (Ushiki, 1986; Kato, 1997). Indeed, our results show that the FTY720-mediated blockade of the S1P-dependent egress results in the accumulation of mature thymocytes even in the perivascular space that is localized in the medulla of normal mice (Figure 3C), supporting the possibility that the medullary perivascular space is a route for the S1P-dependent T cell egress from the thymus in normal mice. Interestingly, however, in mice deficient in CCR7 or CCR7L, the FTY720 treatment accumulates most mature thymocytes in the cortex rather than in the medulla. The accumulation in these mutant mice is detected even in the perivascular space within the cortex (Figure 3C). These results not only reinforce the possibility that the cortex is capable of supporting T cell export, but also support the possibility that the perivascular space within the cortex can serve as a route for the S1P-dependent egress of mature thymocytes. Thus, our results suggest that the cortex-to-medulla migration of developing thymocytes may not be required for the further maturation of thymocytes or for the export of mature thymocytes.

The possibility that similar to the medulla, the cortex can support the generation and export of mature SP thymocytes prompts us to question why the maturation

and 4 show the representative areas of cortical PVS in +/P mice, medullary PVS in +/P mice, cortical PVS in P/P mice, and medullary PVS in P/P mice, respectively. Arrows in the high-magnification images (1–4) indicate the representative PVSs, which are also schematically depicted in the right panels. Shown are representative results of more than ten independent analyses.

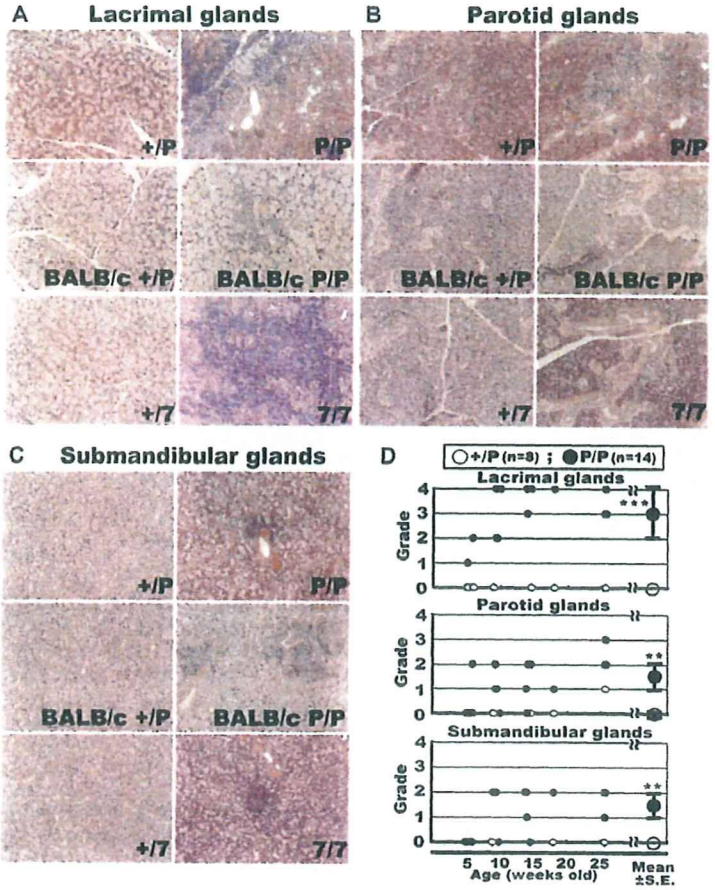

Figure 5. CCR7- or CCR7L-Deficient Mice Exhibit Lymphocyte Infiltration in Lacrimal and Salivary Glands with Tissue Damage

Representative hematoxylin- and eosin-stained tissue sections of lacrimal glands (A), parotid glands (B), and submandibular glands (C) from CCR7L-deficient mice (*plt/plt*, P/P), CCR7-deficient mice (7/7), and their heterozygous control mice (+/P and +/7) are shown. Where indicated, the sections were obtained from *plt/plt* (P/P) and *+/plt* (+/P) mice of BALB/c background.

(D) Histological grading of inflammatory lesions in *plt/plt* (P/P; closed circles) and *+/plt* (+/P; open circles) mice at the indicated age was performed as described in the Experimental Procedures. Double asterisk indicates $p < 0.005$ and triple asterisk indicates $p < 0.0005$ by the Mann-Whitney test.

and export of SP thymocytes in normal mice occur predominantly in the medulla rather than in the cortex. In agreement with previous reports (Matloubian et al., 2004; Allende et al., 2004), our results show that S1P1, the receptor for S1P in T cells, is expressed predominantly by $CD62L^{high}CD69^{low}$ mature SP thymocytes rather than by the less immature thymocytes, including DN, DP, and $CD62L^{low}CD69^{high}$ SP cells. It is therefore likely that most thymocytes, including the DN and DP immature cortical thymocytes as well as the $CD62L^{low}CD69^{high}$ semimature SP thymocytes, are not attracted to S1P, even though neighboring vasculatures in the cortex may supply a gradient of S1P toward the circulation. On the other hand, positively selected DP thymocytes begin expressing a low level of CCR7 (Ueno et al., 2004), and CCR7 is clearly expressed on the positively selected thymocytes at the semimature $CD62L^{low}CD69^{high}$ SP thymocyte stage (Figure 1). Thus, it is likely that in normal mice, positively selected thymocytes in the cortex are attracted to CCR7L, which is predominantly expressed in the medulla, but not attracted to S1P, which penetrates from the vasculature even in the cortex, so that the majority of the positively selected thymocytes are attracted to and accumulated in the medulla. Upon completion of thymocyte differentiation, the S1P1-expressing mature SP thymocytes may be exported to the circulation via the perivascular space within either the medulla or the cortex.

It is also interesting to note that $CD62L^{+}$ cells are sparsely found in the cortex, rather than in the medulla, of the normal untreated mice (Figure 3A), in agreement with previous reports (Reichert et al., 1984; Fink et al., 1985). It was reported that $CD62L^{+}$ cortical thymocytes in normal untreated mice are generated before birth and contain immature DN cells (Reichert et al., 1986a, 1986b), whereas $CD62L^{high}$ mature SP thymocytes are rare in untreated mice and are increased in number upon FTY720 treatment within the medulla of normal mice (Figures 2C and 3A). The developmental status, particularly the significance in thymocyte export, of the $CD62L^{+}$ cells visualized in the cortex of normal untreated mice is still unclear and warrants further analysis.

Medulla Migration and Central Tolerance

Our results show that CCR7- or CCR7L-deficient mice exhibit autoimmune dacryoadenitis and sialadenitis with antibody deposit and tissue damage and that this exocrinopathy is reproduced in lymphocyte-lacking RAG2-deficient mice that are transferred with thymocytes from CCR7L-deficient mice. These results indicate that the thymocytes that are generated without CCR7 signals do not fully establish self-tolerance to the organs, such as lacrimal and salivary glands. Because thymocytes that develop in CCR7- or CCR7L-deficient mice fail to accumulate in the medulla and may be exported directly from the cortex, and because $AIRE^{+}$ cells in the

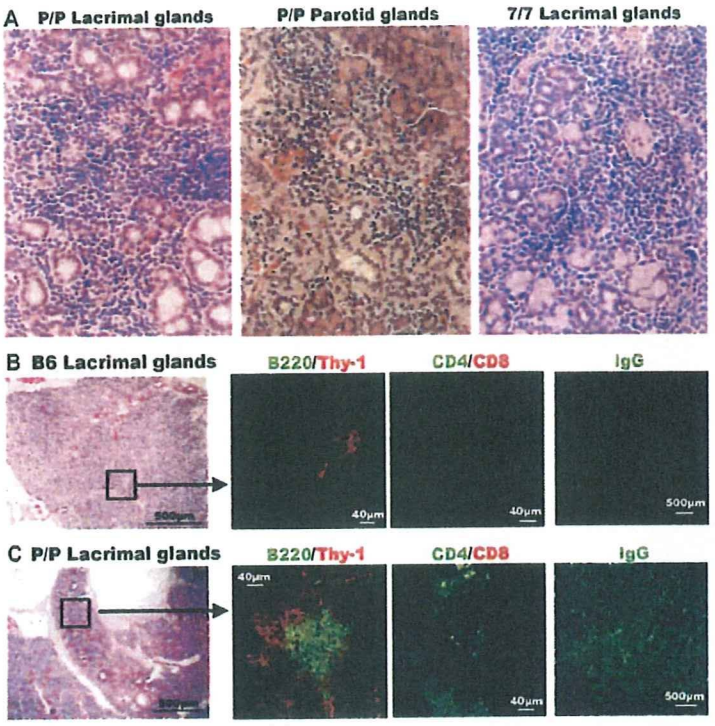

Figure 6. CCR7- or CCR7L-Deficient Mice Exhibit Autoimmune Exocrinopathy

(A) Representative sections of indicated exocrine glands from CCR7L-deficient *plt/plt* mice (P/P) and CCR7-deficient mice (7/7) show that acinar cells in the lacrimal and parotid glands are definitively destoyed in the mutant mice, presenting clear evidence of tissue damage in the mutant mice.

(B and C) Serial sections of lacrimal glands from B6 mice (B) and CCR7L-deficient *plt/plt* mice (P/P) (C) were stained with hematoxylin and eosin or with indicated antibodies. Antibodies used were specific for B220 (green), Thy-1 (red), CD4 (green), CD8 (red), and IgG (green). Shown are representative results of four independent analyses.

thymus are predominantly confined within the medulla even in CCR7- or CCR7L-deficient mice, it is possible that the thymocytes generated in CCR7- or CCR7L-deficient mice are unable to establish self-tolerance to a spectrum of organ-specific antigens because the developing thymocytes fail to interact with AIRE$^+$ mTEC localized in the medulla.

It is interesting to note that similar to CCR7- or CCR7L-deficient mice, AIRE-deficient mice as well as AIRE-deficient APECED patients manifest autoimmune dacryoadenitis and sialadenitis (Anderson et al., 2002; Liston et al., 2003; Kuroda et al., 2005), suggesting that a similar mechanism for the breakdown of central tolerance may be involved in the autoimmunity in these cases. The autoimmune phenotype in CCR7- or CCR7L-deficient mice is mild and restricted to lacrimal and salivary glands. It has been reported that the autoimmune phenotype in AIRE-deficient mice of C57BL/6 background is also mild, being largely limited to lacrimal and salivary glands (Jiang et al., 2005; Kuroda et al., 2005). Thus, the autoimmune phenotype in CCR7- or CCR7L-deficient mice and in AIRE-deficient mice is similarly mild and similarly restricted to lacrimal and salivary glands, at least in the C57BL/6 background. Whether or not the autoimmune phenotype in CCR7- or CCR7L-deficient mice of other genetic backgrounds, particularly the autoimmune-prone NOD background, may be broader and more severe, similar to the phenotype of AIRE-deficient mice, is still unclear and will be addressed in a separate study.

Nonetheless, AIRE-deficient mice of different genetic backgrounds as well as many APECED patients manifest autoimmunity with a spectrum that appears much wider than dacryoadenitis and sialadenitis in CCR7- or CCR7L-deficient mice of the C57BL/6 background (Nagamine et al., 1997; Aaltonen et al., 1997; Anderson et al., 2002; Jiang et al., 2005). It was recently shown that central tolerance to organ-specific antigens is induced not only directly by mTEC antigen presentation but also indirectly by bone-marrow-derived antigen-presenting cells such as DCs (Gallegos and Bevan, 2004). Our results show that DCs in the thymus of CCR7- or CCR7L-deficient mice are normally distributed in the cortex as well as in the medulla (Figure 4). Thus, the more restricted autoimmunity in CCR7- or CCR7L-deficient mice may be due at least in part to central tolerance to DC-mediated crosspresentation of a fraction of AIRE-dependent, organ-specific antigens expressed by mTEC. The milder autoimmunity in CCR7- or CCR7L-deficient mice than in AIRE-deficient mice may also be affected by the compromised immune responses in CCR7- or CCR7L-deficient mice, which are caused by the delayed lymphocyte homing to secondary lymphoid organs (Forster et al., 1999), even though our results show that the similarly mild autoimmune exocrinopathy is caused even in RAG2-deficient mice reconstituted with *plt/plt* thymocytes (Figure 7) in which CCR7/CCR7L signaling in peripheral mature T cells would exhibit no or little aberrancy. How the autoimmunity in CCR7-, CCR7L-, or AIRE-deficient mice is limited to dacryoadenitis and sialadenitis in the C57BL/6 background is still unclear.

We think it is possible that the clonal deletion of self-reactive thymocytes that are specific for a spectrum of organ-specific antigens may be affected in CCR7- or CCR7L-deficient mice, because the thymocytes from these mutant mice exhibit a significantly higher autologous mixed lymphocyte reaction than those from

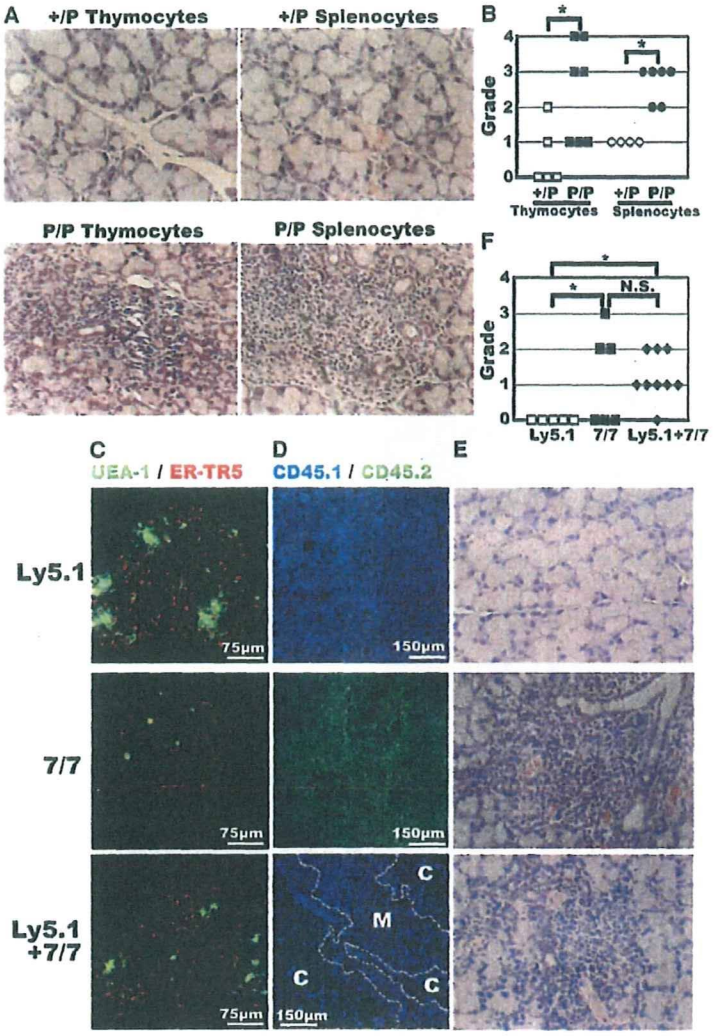

Figure 7. Exocrinopathy Is Associated with Defective Medulla Accumulation of Thymocytes

(A and B) Thymocytes generated in CCR7L-deficient mice are potent in inducing dacryoadenitis and sialadenitis. Thymocytes and splenocytes from CCR7L-deficient *plt/plt* mice (P/P) or control *+/plt* mice were transferred into nonirradiated RAG2-deficient mice. Histopathological analysis was carried out 6 weeks after the cell transfer. Tissue sections of lacrimal glands were stained with hematoxylin and eosin (A), and histological grading was performed as described in the Experimental Procedures (B).

(C–F) T cell-depleted bone marrow cells from B6.SJL-Pt_{prc^a} mice (Ly5.1; $CD45.1^+CD45.2^-$) and/or CCR7-deficient mice (7/7; $CD45.1^-CD45.2^+$) were transferred into nonirradiated RAG2-deficient mice. Where indicated, equal numbers of T cell-depleted bone marrow cells from B6.SJL-Pt_{prc^a} mice and CCR7-deficient mice were transferred (Ly5.1+7.7). Histological and flow cytometry analyses were carried out 6–8 weeks after the cell transfer. The thymuses were analyzed with multicolor confocal microscopy (C) and flow cytometry (data not shown). The UEA-1 and ER-TR5 two-color staining profiles indicate that clusters of $UEA\text{-}1^+$ cells in the medulla are generated in the B6.SJL-Pt_{prc^a} bone marrow chimeras (Ly5.1) and the mixed bone marrow chimeras (Ly5.1+7/7) but are defective in the CCR7-deficient bone marrow chimeras (7/7) (C). Flow cytometry analysis indicated that every mouse used for the analysis exhibited successful thymocyte reconstitution ($2.0–2.5 \times 10^8$ cells per mouse) and that the ratio of $CD45.1^+CD45.2^-$ thymocytes to $CD45.1^-CD45.2^+$ thymocytes in the mixed bone marrow chimeras was in the range of 40:60 to 60:40 (data not shown). The CD45.2 and CD45.1 two-color confocal analysis of the thymus sections (D) along with the staining of the adjacent sections with mTEC-specific ER-TR5 and UEA-1 indicates that $CD45.1^-CD45.2^+$ CCR7-deficient thymocytes are arrested in the cortex (C) and are defective in accumulating in the medulla (M) of the mixed bone marrow chimeras. Tissue sections of lacrimal glands were stained with hematoxylin and eosin (E), and histological grading was performed as described in the Experimental Procedures (F). Asterisk indicates $p < 0.05$ by the Mann-Whitney test; N.S., not significant.

normal mice (H.K. and Y.T., unpublished data), because the mixed bone marrow chimeras reconstituted with bone marrow cells from CCR7-deficient mice and normal mice exhibit the autoimmune exocrinopathy (Figure 7) and because AIRE-expressing mTEC are shown to regulate the deletion of forbidden thymocyte clones (Liston et al., 2003) rather than the generation of regulatory T cells (Anderson et al., 2005). We are currently analyzing whether the clonal deletion of organ-specific-antigen-reactive thymocytes and/or the generation of regulatory T cells may be defective in the thymus of CCR7- or CCR7L-deficient mice.

We have previously reported that negative selection is normally induced in male antigen-specific thymocytes in HY-TCR-transgenic mice and in allogeneic MHC-specific thymocytes in 2C-TCR-transgenic mice even in the absence of CCR7L (Ueno et al., 2004), indicating that negative selection to systemically ubiquitous antigens is normally induced in the absence of CCR7 signals. Perhaps, negative selection to ubiquitous antigens occurs in the cortex without migration to the medulla. We have also shown that Mtv-specific deletion of $V\beta3^+$ and $V\beta5^+$ thymocytes is normally induced in CCR7L-deficient mice (Ueno et al., 2004). It has been reported that DCs in the thymus are primarily responsible for negative selection of Mtv-reactive thymocytes (Moore et al., 1994; Ferrero et al., 1997). Our results show that in CCR7- or CCR7L-deficient mice as well as in normal